Fall 2014

Analysis and practical considerations in implementing multiple transmitters and receivers for wireless power transfer via coupled magnetic resonance

Rizal Johari
Purdue University

PURDUE UNIVERSITY
GRADUATE SCHOOL
Thesis/Dissertation Acceptance

This is to certify that the thesis/dissertation prepared

By Rizal Johari

Entitled
Analysis and Practical Considerations in Implementing Multiple Transmitters and Receivers for Wireless Power Transfer via Coupled Magnetic Resonance

For the degree of   Doctor of Philosophy

Is approved by the final examining committee:

JAMES V. KROGMEIER

DAVID J. LOVE

MARK R. BELL

XIAOJUN LIN

To the best of my knowledge and as understood by the student in the Thesis/Dissertation Agreement, Publication Delay, and Certification/Disclaimer (Graduate School Form 32), this thesis/dissertation adheres to the provisions of Purdue University's "Policy on Integrity in Research" and the use of copyrighted material.

JAMES V. KROGMEIER

Approved by Major Professor(s): _____

Approved by: V. Balakrishnan   12/05/2014

Head of the Department Graduate Program   Date

ANALYSIS AND PRACTICAL CONSIDERATIONS IN IMPLEMENTING

MULTIPLE TRANSMITTERS AND RECEIVERS FOR WIRELESS POWER

TRANSFER VIA COUPLED MAGNETIC RESONANCE

A Dissertation

Submitted to the Faculty

of

Purdue University

by

Rizal Johari

In Partial Fulfillment of the

Requirements for the Degree

of

Doctor of Philosophy

December 2014

Purdue University

West Lafayette, Indiana

ACKNOWLEDGMENTS

I would like to express my utmost gratitude to my adviser, Prof. James Krogmeier, who has provided immense guidance, advice and friendship in my years as a graduate student. He has always believed in me and continued to provide motivation to always be a better researcher and person. Special thanks to Prof. David Love, who is on my committee for his insightful comments and tutelage. I would also like to thank Prof. Mark Bell and Prof. Xiaojun Lin for their continuing support and advice as members of my doctoral committee.

To my fellow lab mates from both TASC and CRL, thank you for the countless discussions and conversations which have directly or indirectly impacted my research and my life. The years of friendship and hardship together have been a great and meaningful journey.

I was very fortunate to have had the mentorship of Barrett Robinson and Matthew Swabey through my teaching assistantship. The lively discussions we had were truly motivational and inspiring.

To Abg. Fikri, Kak Nana, Faiz and Awil, you are like family to me. Thank you so much for your support and prayers. To my friends Tonjang and Shida, thank you for the continued friendship. It has been a blessing to see our families grow together. To our close friends at Purdue, Gurnee, Boston and the Bay Area community, I am thankful to have such amazing and wonderful friends. If you are reading this, you are one of those people.

Mom and Dad, thank you so much for your unconditional love and support. I would not be where I am today without you. Also to my brothers, Johann and Adam, who have been there for me throughout the years. To my in-laws, Mak and Ayah, and sister-in-laws, I am grateful for your continued support and love.

Last but not least, I cannot even begin to describe the amount of support and encouragement my loving wife, Farah and daughter, Arianna have given me. They are the pillar of my strength and focus.

TABLE OF CONTENTS

LIST OF TABLES

LIST OF FIGURES

ABBREVIATIONS

TX	Transmitter
RX	Receiver
CMR	Coupled Magnetic Resonance
RMS	Root Mean Square
SISO	Single-Input Single-Output
SIMO	Single-Input Multiple-Output
MISO	Multiple-Input Single-Output
TDM	Time Division Multiplexing
ADS	Advanced Design System
SNR	Signal to Noise Ratio
PLC	Power Line Communication
AWGN	Additivie White Gaussian Noise
CMT	Coupled Mode Theory
WPT	Wireless Power Transfer

ABSTRACT

Johari, Rizal Ph.D., Purdue University, December 2014. Analysis and Practical Considerations in Implementing Multiple Transmitters and Receivers for Wireless Power Transfer via Coupled Magnetic Resonance. Major Professor: James V. Krogmeier.

The technology to wirelessly power mobile devices has started to gain momentum especially in industry. Cables have started to become the thing of the past as both wireless power efficiency and communication speeds become viably attractive. The first part of this work gives analysis and practical considerations in implementing multiple transmitters for wireless power transfer via coupled magnetic resonance. Through the multiple transmitter scheme, there is an increase in gain and diversity of the transmitted power according to the number of transmit coils. The effect of transmitter resonant coil coupling is also shown. Resonant frequency detuning due to nearby metallic objects is observed and the extent of how much tuning can be done is demonstrated. A practical power line synchronization technique is proposed to synchronize all transmit coils. This reduces additional dedicated synchronization wiring or the addition of an RF front end module. The second part of this study introduces a time division multiplexing (TDM) technique for tightly coupled receivers via the same method of coupled magnetic resonance. Two or more receivers can be powered simultaneously using a single transmit coil. In a tightly coupled receiver scenario, the received power is significantly reduced. Experimental and simulation results implementing TDM show vast improvements in received power in the tightly coupled case. Resonant frequency splitting is eliminated through synchronized detuning between receivers, which divide power equally between receivers at specific time slots. The last chapter gives insight on the capacity of a single-input single-output

system at varying distances between receiver and transmitter. It is shown that the highest information rate is achieved at critical coupling.

1. INTRODUCTION

1.1 Introduction to wireless power
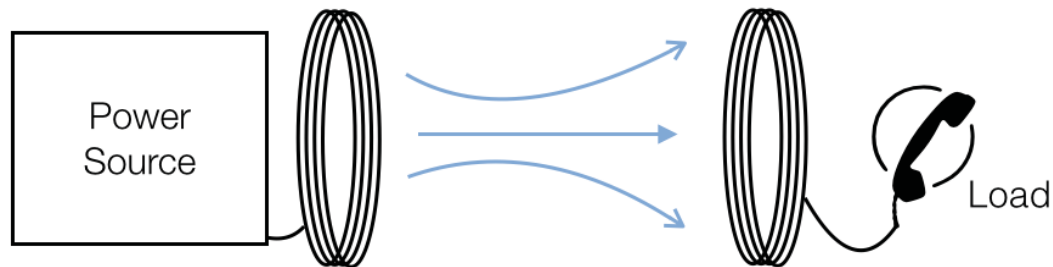
Fig. 1.1. The inductive wireless power transfer method

Wireless power transfer is described as the transmission of electrical energy from a power source to a load without the use of a physical connection. An example of an early product which utilized inductive or magnetic fields to transfer power is the electric tooth brush. Even though the distance has to be very close between receiver and transmitter, it provides an enclosed casing which prevents accidental electric shock due to water seepage. One can think of an air coil transformer with a primary and secondary winding. Instead of having a ferrite core to help concentrate magnetic fields, the design of the product requires very close distances to ensure a high coupling coefficient. The problem with inductive transfer is primarily due to the requirement of having very close distances between receiver and transmitter. Fig. 1.1 shows a basic diagram of an inductive wireless charging system.

A lot of progress has been made to increase distance, efficiency and orientation flexibility through different approaches or technologies. They include laser, radiowave, capacitive coupling, and in this work, coupled magnetic resonance. The advantages of using laser or radiowave transmissions is the ability to transmit power at very

long distances. However, it requires a very complex tracking algorithm because line-of-sight is needed and can be easily obstructed by buildings, trees, etc. Capacitive coupling on the other hand behaves similarly to the inductive method but requires dangerously high voltage swings in terms of electric fields which can harm living organisms. Magnetic fields on the other hand does not react to human or animal tissue, which behaves like water content with extremely low interactions. Most, if not all consumer devices that have wireless power capabilities, use magnetic field induction as the transfer technology. In this work, a coupled magnetic resonance method is used as it enables medium range transfer distances and orientation flexibility at a much lower coupling coefficient between transmitter and receiver when compared to the inductive method.

1.2 Coupled magnetic resonance

The concept of coupled magnetic resonance is the addition of extra resonant coils at each transmitter and receiver units depicted in Fig. 1.2. Its resonance is tuned to the same source frequency. Coupled magnetic resonance is an inductive type coupling system which uses the resonant coil as the main point of interaction between source and load.
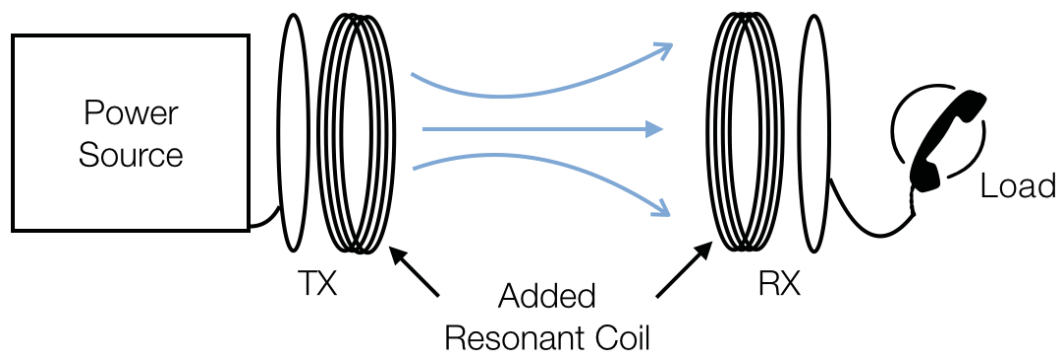
Fig. 1.2. An illustration explaining the concept of coupled magnetic resonance

1.3 Practical considerations for wireless power transfer using multiple transmitters

Recently, there has been significant interest in efficient medium-range wireless power transfer for powering and/or charging future personal electronic devices. Systems that allow short-range powering and charging are already commercially available and research challenges remain in extending the range and improving the power transfer efficiency. Researchers have demonstrated that inductive coupling between low-loss resonant coils allows significant power to be transmitted with high efficiency over distances on the order of a few times the radius of the transmit coil [3], [4]. The single transmitter (TX) and single receiver (RX) demonstration system consists of four coils, two at the TX and two at the RX. The two coils at the power transmitter consist of a source coil and a resonant coil. Similarly, the two coils at the power receiver consist of a resonant coil and a load coil.

Applications for medium range wireless power transfer could include a wide range of areas, among them are wireless controlled robots, RFID based systems [8], electric vehicle charging [10], charging mobile devices and biomedical implants [8], [15]. Different system configurations such as a multiple receiver setup where a single transmit coil powers several loads have been discussed in [6], [9]. The coupling coefficients linking each resonant coil, which corresponds to the geometry, angle and distance between coils play an important role in transmission efficiency. Reference [16] introduces an adaptive frequency technique to ensure maximum power transfer efficiency within an overcoupled region where frequency splitting occurs. In [17], the distance between TX/RX coil pairs are adjusted to keep an effective 'matching condition'. Power transfer efficiency for multiple transmitters in a fixed position surrounding the load is investigated by [14]. Their test case shows a theoretical bound on power transfer efficiency for the 2 TX and 1 RX case. Effect of coupling between multiple transmitters or receivers for the single resonant source/load coil configuration is discussed in [11]. Multiple transmitters using an optimized structure is used by [25] to

maximize coupling between TX and RX for a free-positioning planar system. Coupled magnetic resonance can further be extended to increase the operating distance by introducing relays [5], [7], [12]. An increased gain is seen at further distances due to efficient wireless energy transfer between relay coils.

References [3]- [7] use coupled mode theory (CMT) as an analytical framework to model resonant energy exchange. Our work relies on basic circuit theory to model the resonant energy transfer, as also done in [9]- [19]. As proved in [21], both frameworks result in the same set of equations in steady state and are applicable for both short and midrange coupling conditions.

1.4 Time division multiplexing for tightly coupled receivers

The adoption rate for wireless charging applications have increased exponentially with major cell phone manufacturers adopting the Qi wireless power standard [35]. The capability of charging devices seamlessly by simply placing it on a table at a designated charging area seems very desirable and simple. As more devices incorporate the ability to charge wirelessly, there is a need for charging devices simultaneously using the same power source (TX). However, there are certain issues when multiple receivers are clumped closely together. Coupling between receivers induce frequency splitting and ultimately reduces the efficiency and power received. A practical time division multiplexing (TDM) technique is proposed to eliminate receiver coupling. A circuit model using a one transmit and two receive coil setup is developed and compared to the experimental measurements. Resonant frequency splitting is eliminated through synchronized detuning between receivers. Equal power is distributed between receivers at their own unique receiver time slot.

Methods for enhancing charging distance face numerous challenges, especially when charging multiple devices. To increase freedom of movement, an extra resonator coil is placed at both transmitter (TX) and receiver (RX) [3]. This technique increases the Q-factor of the resonator coil by separating the source and load impedances to

generate increased current flow. However, this increases the resonator coil's sensitivity to nearby equivalent resonators. The transfer function of the system operates in a narrow frequency range due to the coil's high Q properties. Slight shifts in the coil's inductance can dramatically reduce received power. This applies to both TX and RX coils.

Practical applications for a multiple receiver case include powering and/or charging multiple mobile devices simultaneously. Devices include cell phones, tablets, laptops, biomedical equipment, etc. The ability to operate with loosely coupling conditions enable the possibility of placing physical charging pads obscurely underneath tables, behind walls, or under concrete. This helps reduce clutter and adds mobility improvements in terms of device orientation and charging area. The concept of coupled magnetic resonance (CMR) was first introduced in [3], [4]. Work in [9] discussed multiple receiver frequency splitting when two receivers are tightly coupled. Reference [11] discusses a general framework for the behavior of multiple transmitter and receiver coupling. CMR has already been used in a wide array of applications including charging electric vehicles [18], biomedical implants [15], and wireless power transfer relays [5] to powering sensors in nuclear waste management [31].

Early research [16], [19], [32], [13] mostly concentrated on single transmit and single receive, i.e., single-input single-output (SISO), applications to improve power and efficiency with respect to tight, loose or critical coupling. There has been increased interest in incorporating multiple transmitters [1] and receivers [30] which add the benefits of increased power, diversity, and simultaneous powering capabilities. An overview of multiple receiver concepts is found in [33].

The two receiver case with tight coupling, corresponding to very close distance between receiver coils, experiences a reduction in induced current due to opposing magnetic flux cancellation in both coils. The effective mutual inductance results in frequency splitting affecting both efficiency and power transfer functions. A time division multiplexing (TDM) technique is introduced to improve power transfer at positions that exhibit very tight coupling and is activated to allow charging at one

receiver during its exclusive time slot. This is achieved by detuning the neighboring coil and is electrically invisible to the system. The WPT system used in this work uses TX and RX coils that are resonantly tuned to the driving frequency. Work in [30] uses a multiple receiver setup that has different receiver coil resonance and shows that the efficiency follows the receiver's characteristics regardless of the TX. However, the amount of power transferred is severely limited if the TX coil resonance characteristics do not match the source frequency.

The A4WP group [34] has demonstrated CMR-type, i.e., loose coupling between TX and RX concepts and can support up to three devices simultaneously. Minimizing coupling between CMR receiver devices becomes important when compared to a non-resonant or single resonant coil method. Using TDM, the number of devices in close proximity being charged can be increased, at the expense of a penalty incurred in transmitted power due to time allocation between devices. Enhancements can be made such that only tightly coupled RX devices undergo TDM while devices being loosely coupled are charged simultaneously.

1.5 Future Work: Simultaneous power and information transfer tradeoff analysis

Interest in wireless power and information transfer has increased significantly. Extensive research studies are being done to improve wireless power transfer while also having the ability to communicate using the magnetic coupling channel between the power source and receiving device. Due to the various needs of having improved power efficiency and spatial freedom in terms of distance and orientation, a number of wireless power transfer schemes have been developed. They include inductive , resonant-inductive and coupled magnetic resonance inductive charging systems. There are tradeoffs to the various wireless power transfer schemes that are in existance today. All of the schemes have been deisgned for optimal wireless power transfer and not many have studied the information rate associated with such schemes. Concessions

can be made to reduce power transfer with the intent of increasing information rate. The capacity for the single-input single-output coupled magnetic resonance system is studied at different coupling distances.

One can take a power-centric approach of focusing only on increased power transfers with reduced communication. There is a tradeoff between having maximum transferred power with the information rate as power transfer is maximized at the single sinusoidal resonant frequency. The size of the bandwidth is inversely proportional to the amount of power transferred. Early work done by [36] was the first to consider the problem of information and power transfer tradeoffs of an inductively coupled system. If a system is ran at near capacity, security measures that can detect eavesdropping through detuning was discussed by [41]. Capacity and link budget analysis at different Q values for the transmitter and receiver for an inductive communication system was explained in [42]. The inductively coupled wireless power system is modeled as a frequency selective channel with additive white Gaussian noise (AWGN). The frequency selective channels are based on the efficiency function of the system and are chosen to have small bandwidth bins. It is shown in this work that the highest information rate is achieved at critical coupling.

1.6 Organization

This dissertation is organized as follows. In Chapter 2, analysis and practical considerations in implementing multiple transmitters is described. The basic principles and framework for a two transmitter and one receiver case is explained in Section 2.1. In Section 2.2, the transfer function for the multiple transmitter case is simulated and compared with actual measurements. Effects of transmitter resonant to resonant coupling are analyzed in Section 2.3. Section 2.4 explains the diversity effect and is shown by incidental resonant frequency shifts due to nearby metallic objects. The last part of Chapter 2 gives details of a practical synchronization technique via power line communications including its benefits.

Chapter 3 describes a time division multiplexing wireless power transfer method for tightly coupled receivers. An introduction to multiple receivers is discussed in Section 3.1. Section 3.2 describes the basic principles and framework for TDM and a one transmitter and two receiver WPT setup. In Section 3.3, the initial proof-of-concept was simulated using Advanced Design System (ADS) before beginning experimental work. The TDM implementation circuitry and concept is presented in Section 3.4. Section 3.5 presents simulation and experimental results with and without TDM implementation including strategies for determining when to activate TDM. Lastly, Section 3.6 discusses TDM enhancements and future work.

Future work regarding tradeoff analysis of simultaneous power and information transfer is discussed in Chapter 4. To conclude, Chapter 5 provides a summary of all the work done.

2. ANALYSIS AND PRACTICAL CONSIDERATIONS IN IMPLEMENTING MULTIPLE TRANSMITTERS

2.1 Multiple transmitter system overview

Different scenarios constitute different setups in a wireless power transfer scheme. The focus in this chapter is to utilize more than one TX coil pair for added gain and diversity benefits. There are certain challenges when using multiple coils which include signal synchronization and coupling between multiple transmitters. By increasing the number of transmitters, power transfer reliability and gain can be improved while also regulating the amount of power being sent through free space. Metal object interference or the ability to uniformly send power over a wide area can be supported by having synchronized transmitters.
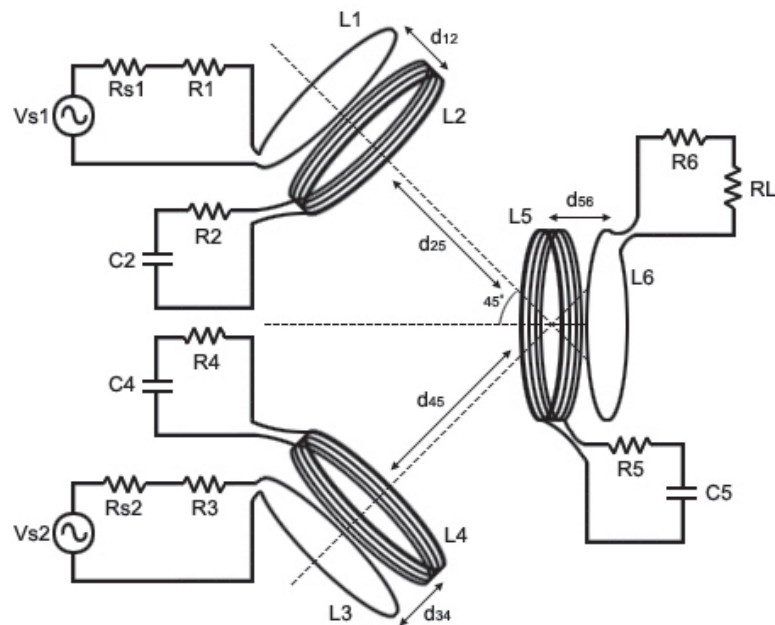
Fig. 2.1. Two transmitter and one receiver experimental setup.

Fig. 2.1 illustrates the experimental setup for 2 TX pairs and one RX pair. This setup assumes loose coupling between both TX coils and also the RX pair coils. If the TX and RX coils are tightly coupled, frequency splitting occurs and would degrade the efficiency of the system. Frequency adaptation [16], variable coupling between coil pairs [17], matching networks [26] or antiparallel resonant loops [27] could be used to improve efficiency at these distances. These techniques can be used in the multiple transmitter case considering loose coupling between transmitter resonant coils and equal distance between both TX and RX coils.

Source voltages V_{S1} and V_{S2} in Fig. 2.1 are sinusoidal signals with equal magnitude and phase. A total of 6 inductor coils labelled L_1 through L_6 with radii of 0.057 m were constructed using AWG14 copper magnet wire. The resonator coils in this setup have 5 turns each. For simplicity, the source and load coils consist of only 1 turn. The distances, d_{12}, d_{34}, and d_{56} between coil pairs were set at 0.04 m. The transmitters were placed at a distance, $d_{25} = d_{45} = 0.35$ m away from the receiver with angular separation of 45°. Resistances R_1 through R_6 are the coil's ohmic resistance at resonance. R_{S1} and R_{S2} represent the source resistances and R_L is the load resistance. The resonant coils L_2, L_4, and L_5 were terminated with lumped capacitors C_2, C_4 and C_5, whose values were chosen such that the resonant frequencies

$$f_0 = \frac{1}{2\pi\sqrt{LC}} \tag{2.1}$$

were all equal. It is important that the driving signals at each source be synchronized with the same frequency and phase in order to avoid severe power fluctuations at the receiver. Capacitances C_2, C_4 and C_5 are the sum of parasitic capacitance (C_P) between the turns of the multi-turn resonant coils and lumped capacitance (C_L) included for tuning the resonant frequency ($C_i = C_{i,P} + C_{i,L}$, for $i = 2$, 4, and 5). Since the resonant coils were designed to have high Q, it is important to account for parasitic capacitance. Small offsets of $1 - 2$ pF (parasitics) can cause a resonant shift of approximately $70 - 150$ kHz and with a very narrow bandwidth even the slightest shift can degrade performance. The parasitic capacitance for coils L_1, L_3 and L_6 are neglected since they have but a single turn.The resonator coils L_2, L_4, and L_5 have the

same nominal inductances since they are identically fabricated. The coils were tuned to the selected driving frequency of 8.4 MHz by adjusting the lumped capacitors $C_{i,L}$. Assuming sinusoidal steady state excitation the phasor voltage across the k-th coil
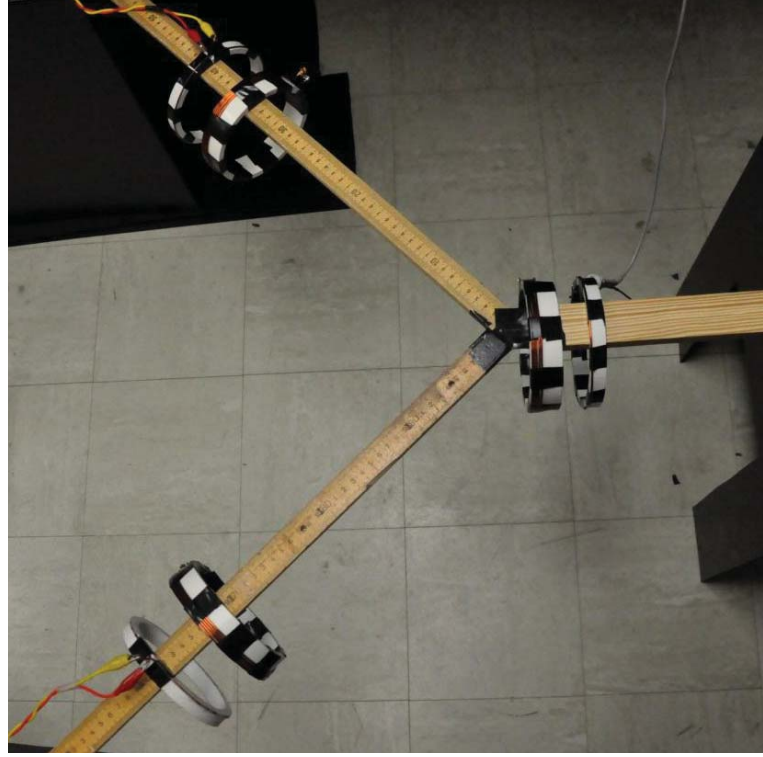
Fig. 2.2. A picture of the 2-TX and 1-RX wireless power transfer system experimental setup.

can be written as $V_{coil,k} = j\omega\Delta_k$ where

$$\Delta_k = L_k I_k \pm \sum_{l \neq k} M_{k,l} I_l \tag{2.2}$$

is the total flux linking the turns of the k-th coil, $M_{k,l}$ represents the mutual inductance between coils k and l, and I_l is the phasor current in the l-th coil. $M_{k,l}$ can be expressed in terms of the coupling coefficient $k_{k,l}$ and self inductance of the corresponding loops L_k and L_l as such

$$M_{k,l} = k_{k,l}\sqrt{L_k L_l} \tag{2.3}$$

With the above constitutive equations and Kirchoff's voltage law taken at each loop as depicted in Fig.2.1, one can solve for phasor currents as the product of the inverse of the impedance matrix times a source voltage column vector:

$$
\begin{bmatrix} I_1 \\ I_2 \\ I_3 \\ I_4 \\ I_5 \\ I_6 \end{bmatrix} = \left[\{Z_{k,l}\}_{1 \leq k,l \leq 6} \right]^{-1} \begin{bmatrix} V_{S1} \\ 0 \\ V_{S2} \\ 0 \\ 0 \\ 0 \end{bmatrix} \tag{2.4}
$$

The individual impedances $(Z_{k,l})$ are given by

$$
Z_{11} = j\omega L_1 + R_{S1} + R_1
$$

$$
Z_{22} = j\omega L_2 + R_2 + \frac{1}{j\omega C_2}
$$

$$
Z_{33} = j\omega L_3 + R_{S2} + R_3
$$

$$
Z_{44} = j\omega L_4 + R_4 + \frac{1}{j\omega C_4}
$$

$$
Z_{55} = j\omega L_5 + R_5 + \frac{1}{j\omega C_5}
$$

$$
Z_{66} = j\omega L_6 + R_6 + R_L \tag{2.5}
$$

with $Z_{k,l} = Z_{l,k} = j\omega M_{k,l}$ for $k \neq l$ with the exception of $Z_{x,y} = Z_{y,x} = -j\omega M_{x,y}$ for $\{x, y\} = \{1, 3\}, \{1, 4\}, \{2, 3\}$ and $\{2, 4\}$. Please note that Equation (2.4) is not simplified and represents a complete general solution for finding the corresponding loop current. No simplifying assumptions were made for (2.4) except that the system being linear and time invariant. The result of Equation (2.4) is the superposition for each transmit source with a Z impedance matrix representing all coil interactions detailed in (2.6).
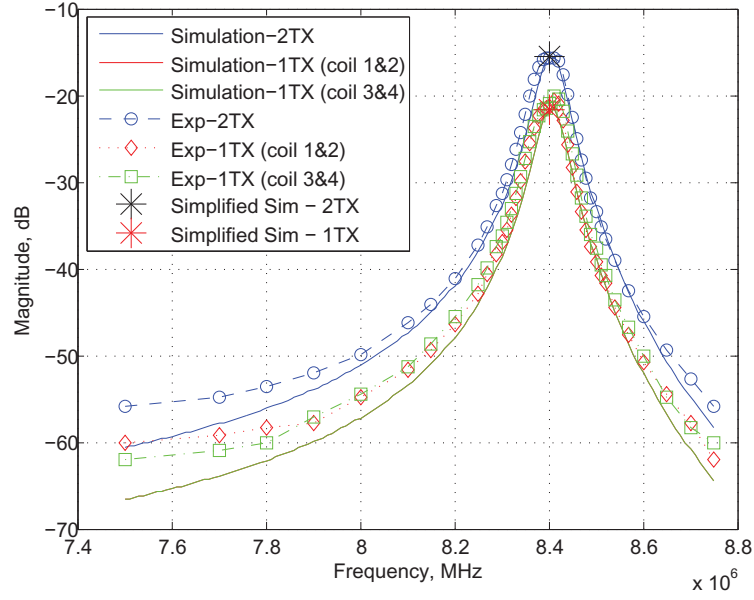
Fig. 2.3. Transfer Function $|V_L/V_s|$ (dB) for simulated (complete and simplified) and experimental measurements for two and one transmitter setups.

$$
\begin{bmatrix} I_1 \\ I_2 \\ I_3 \\ I_4 \\ I_5 \\ I_6 \end{bmatrix} = \begin{bmatrix} Z_{11} & Z_{12} & ... & ... \\ Z_{21} & Z_{22} & & \\ \vdots & & \ddots & \\ \vdots & & & Z_{66} \end{bmatrix}^{-1} \begin{bmatrix} V_{S1} \\ 0 \\ 0 \\ 0 \\ 0 \\ 0 \end{bmatrix} + \begin{bmatrix} Z_{11} & Z_{12} & ... & ... \\ Z_{21} & Z_{22} & & \\ \vdots & & \ddots & \\ \vdots & & & Z_{66} \end{bmatrix}^{-1} \begin{bmatrix} 0 \\ 0 \\ V_{S2} \\ 0 \\ 0 \\ 0 \end{bmatrix}
$$

$$
= \begin{bmatrix} Z_{11} & Z_{12} & ... & ... \\ Z_{21} & Z_{22} & & \\ \vdots & & \ddots & \\ \vdots & & & Z_{66} \end{bmatrix}^{-1} \begin{bmatrix} V_{S1} \\ 0 \\ V_{S2} \\ 0 \\ 0 \\ 0 \end{bmatrix} \tag{2.6}
$$

The magnitude of the load voltage is $|V_L| = |R_L I_6|$ and we wish to compute and compare transfer functions from inputs to the load for both the SISO and MISO case. For simplicity, we assume $V_{S1} = V_{S2} = V_S$ for the MISO case. For the SISO case we can assume without loss of generality that $V_{S1} = V_S$ and $V_{S2} = 0$. In either case we plot transfer functions $|V_L/V_S|$ (dB) vs. frequency.

Solving for I_6 explicitly from (2.4) results in a very complicated expression. To simplify things, with respect to the experimental setup conditions, we can set $Z_{11} = Z_{33}$ due to both source coil's equal properties. The resonator coils also share the same characteristics resulting in $Z_{22} = Z_{44} = Z_{55}$. Cross coupling coefficients are neglected and are set to zero. This results in a simplified impedance matrix as stated in (2.7),

$$
\begin{bmatrix}
Z_{11} & jwM_{12} & 0 & 0 & 0 & 0 \\
jwM_{12} & Z_{22} & 0 & 0 & jwM_{25} & 0 \\
0 & 0 & Z_{11} & jwM_{12} & 0 & 0 \\
0 & 0 & jwM_{12} & Z_{22} & jwM_{25} & 0 \\
0 & jwM_{25} & 0 & jwM_{25} & Z_{22} & jwM_{12} \\
0 & 0 & 0 & 0 & jwM_{12} & Z_{66}
\end{bmatrix}
\tag{2.7}
$$

The above simplification gives us a reasonable model of the experimental setup in Fig. 2.1 where (2.8) is the simplified equation for I_6. The transfer function for the MISO case can be obtained through superposition of the two power sources. At resonance, simulation and theoretical results show no substantial difference in values for I_6 between the simplified equation, $I_{6(a)}$ in (2.8) and the exact one, I_6, in (2.4) when cross couplings are set to zero. The simplification model assumes loose coupling between TX and RX and also both TX.

$$
I_{6(a)} = \frac{jw^3 M_{12}^2 M_{25} \left(A_{S1} e^{j\theta_{S1}} + A_{S2} e^{j\theta_{S2}} \right)}{w^4 M_{12}^4 + Z_{11} Z_{66} Z_{22}^2 + w^2 Z_{11} M_{12}^2 Z_{22} + w^2 Z_{66} M_{12}^2 Z_{22} + 2w^2 Z_{11} Z_{66} M_{25}^2}
\tag{2.8}
$$

Further analysis of (2.8) shows a voltage gain of 2 and a power gain of 4 when the phasor voltage $V_{S1} = A_{S1} e^{j\theta_{S1}}$ and $V_{S2} = A_{S2} e^{j\theta_{S2}}$ are equal in both magnitude ($A_{S1} = A_{S2}$) and phase ($\theta_{S1} = \theta_{S2}$). This is a direct result of $|V_L| = |I_6 R_L|$ and $|P_L| = |I_6^2 R_L|$ when the current of I_6 is doubled. The gain shown above is only true
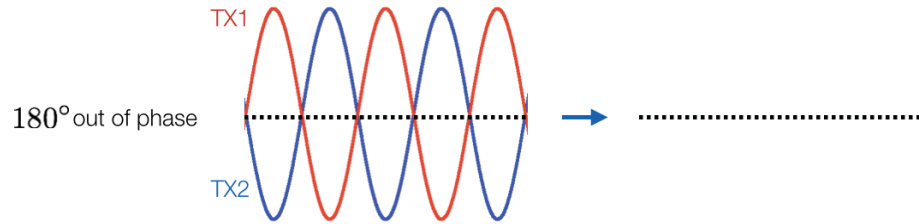
Fig. 2.4. Phase offset of 180° experiences complete destruction with zero output.
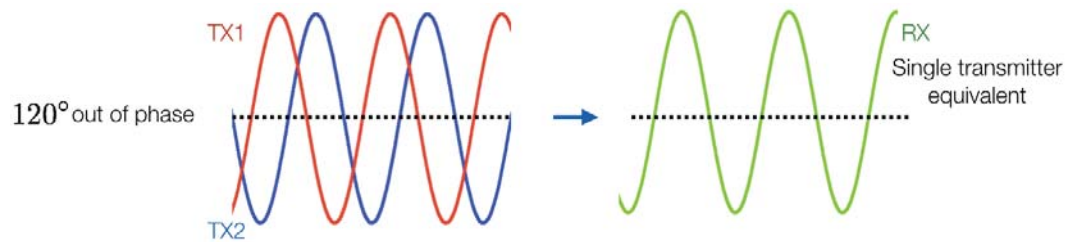
Fig. 2.5. Phase offset of 120° results in an equivalent single-input single-output case in terms of received power.

if the transmitters are synchronized in frequency, phase and amplitude. One can relate the two synchronized transmitters with a single transmitter but with twice the amplitude.

In a practical system, input sources could be out of phase. The difference in phase, results in a lower transfer function value with the worst case at 180°. Total desctructive combining occurs with a zero output value as seen in Fig. 2.4. If both transmitters have an offset of 120°, the combined output is equivalent of the SISO case. Fig. 2.5 shows an output with an equal magnitude sinusoid with a fixed phase offset. If the input signals are completely out of phase, theoretically no power should be transferred due to complete destructive combining at the receiver. Experiments conducted by [22] investigates different receiver angles for two cases involving in-phase and out-of-phase input signals that also show the destructive case at a 0° receiver angle.

2.2 Experimental and simulation results and analysis

Three different measurements were taken with both transmit coils turned on and two measurements taken with the transmit coils turned on individually. This was done to experimentally determine the gain available from using additional transmit coils. The experimental setup assumes static transmitter coil positions with distances large enough to avoid coupling between transmit resonant coils. Fig. 2.2 is an image of how the experiment was set up.

The experimental results agree well with the theoretical results as shown in Fig. 2.3. As explained in Section 2.1, there is a 6 dB gain in theory provided that both signals ideally combine coherently at the receiver. Actual transfer function measurements showed a gain of approximately 5.3dB. This 0.7 dB difference could be due to small matching errors in the coil resonant frequencies, minor phase delay differences between reference signals, and imperfect geometric alignment between transmitter and receiver.

The use of a voltage transfer function was perferred to the power transfer function due to the superposition principle in which the voltage received can be added directly. Previously cited papers [9] and [33] also presented their results in the voltage transfer function format. However, the paper by Sample et al. [16] converts the voltage transfer function to the linear magnitude scattering parameters ($|S_{21}|$ due to its connection with vector network analyzer experimental measurements. The equation used is:

$$S_{21} = 2\frac{V_{Load}}{V_{Source}}\left(\frac{R_{Source}}{R_{Load}}\right)^{1/2} \tag{2.9}$$

Specifically for the multiple transmitter case, the decision to use basic voltage transfer function is due to its ease of voltage addition and comparison.

The benefits of having multiple transmitters considering hardware limitations (limited power or size of transmitter) is that one could increase gain or power transfer area by simply adding extra transmitters. If a larger power transfer area is preferred rather than gain, extra transmitters could be added such that the power transfer is
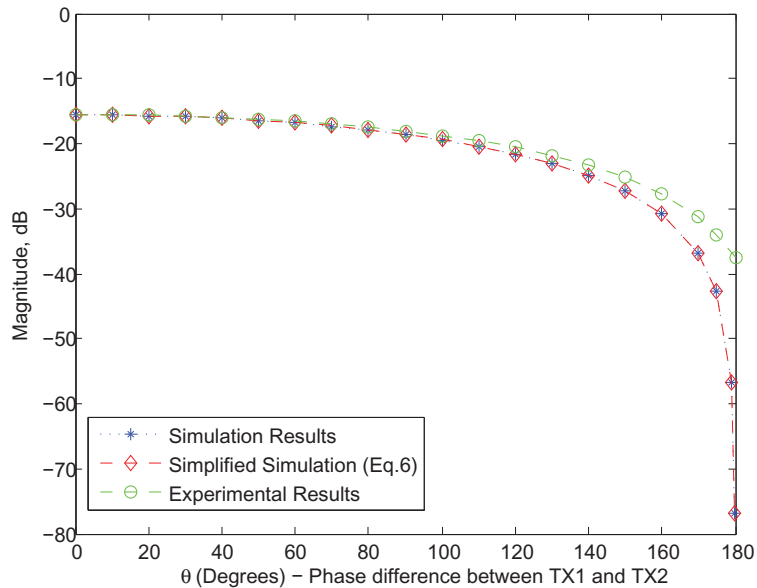
Fig. 2.6. Transfer Function $|V_L/V_s|$ (dB) with phase differences at TX ($\theta - \theta_1$, $\theta_1 = 0°$, f = 8.4MHz).

combined at the edges to ensure uniform gain distribution. A number of difficulties arise with added transmitters including reference signal synchronization and phase delays due to differing distances between the transmit power coils and the receiver coil. It is important to make sure that the shared frequency is locked.

In this work, a master reference signal is shared with the TX coil (slave). This will ensure a locked frequency with slight phase delays depending on the signal wavelength, distance and channel characteristics between TX coils. As seen in Fig. 2.6, at 8.4MHz, a phase difference of 10° between transmitters degrades the voltage transfer function by only 0.38% or 0.03dB while a 90° phase difference results in a 30% or 2.4dB degradation experimentally. In theory, if the phase difference is 120°, the results would be the same as if only one TX was transmitting. For the 180° out-of-phase case, the experimental results show a 99.9% reduction in received voltage which in theory is 100% reduction at zero volts. In practice, complete destructive combining is rarely occurs due to minor differences of the coils Q-factor or resonance, angle

and distance between both TX to the RX. The simulation results for the simplified case (2.8) and the complete case (I_6 in (2.4)) are the same and agree well with the experimental results.

The multiple transmitter setup as shown in Fig. 2.2 uses an on-axis setup where the TX coils are tilted on-axis facing the receiver. An off-axis position such as placing both TX coils in a flat position would provide similar results where the underlying gain and diversity concepts still hold but with reduced coupling coefficient values between TX and RX due to angular orientation. The off-axis case on the other hand provides a more practical scenario such as embedding transmitters within walls. This is particularly useful for a uniform power transfer area while the on-axis case is suited for a localized concentrated power transfer area. Fig. 2.7 illustrates the off-axis case. Research using the on-axis case was chosen because of its simpler relationship to the TX resonant to resonant coupling case when RX and TX angles are reduced from 45° to 10° without changing its distance.

Table 2.1
Parameter Values

Par.	Value	Par.	Value	Par.	Value	Par.	Value
R_{S1}	50 Ω	L_1	.30 μH	k_{12}	.2	k_{34}	.2
R_{S2}	50 Ω	L_2	6.10 μH	k_{13}	.0001	k_{35}	.0006
R_1	.053 Ω	L_3	.30 μH	k_{14}	.0001	k_{36}	.0005
R_2	.265 Ω	L_4	6.11 μH	k_{15}	.0006	k_{45}	.00064
R_3	.053 Ω	L_5	6.12 μH	k_{16}	.0005	k_{46}	.0006
R_4	.265 Ω	L_6	.31 μH	k_{23}	.0001	k_{56}	.2
R_5	.265 Ω	C_2	58.9 pF	k_{24}	.0001		
R_6	.053 Ω	C_4	58.8 pF	k_{25}	.00064		
R_L	100 Ω	C_5	58.7 pF	k_{26}	.0006		
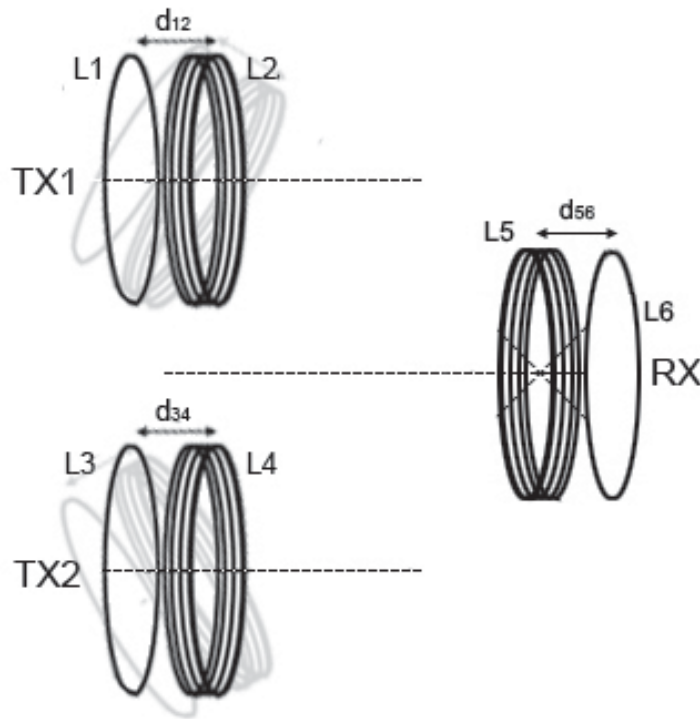
Fig. 2.7. Off-axis phased array situtation by rotating TX1 and TX2.

2.2.1   Parameter Values

The parameter values used in the simulations consist of measured and theoretically calculated values. The self inductances of each coil (L_1 to L_6) were measured using a Sencore LC102 Capacitor-Inductor Analyzer. The AC resistances of the coils were based on the standard formula (which accounts for skin effect),

$$R = \frac{rN}{a} \sqrt{\frac{\omega \mu_0}{2\sigma}} \tag{2.10}$$

where r is the coil radius, N is the number of turns, a is the cross sectional radius of the wire, $\omega = 2\pi f$ is the angular frequency (here corresponding to the nominal resonant frequency of 8.4 MHz), μ_0 is the magnetic permeability of free space ($4\pi \times 10^{-7}$ H/m) and σ is the conductivity of copper (5.813×10^7 S/m). Total capacitance values C_2, C_4 and C_5 for the corresponding resonant loop were computed using measured inductance

values and the formula for resonance in (2.1). The neglected cross coupling coefficients in the previous section were included in the simulation results for a more accurate analysis within a wider frequency range. Coupling coefficient values were chosen to fit the experimental results as was done in [9] and were based on the characteristics of the coil's distance between each other and also their angular orientation. Table 3.3 shows the parameter values used in the experiment and simulations. Simulated SISO conditions for each transmitter were shown in Fig. 2.3 to corroborate the coupling coefficient values. Another method by [13] measured various S-Parameter configuration values and were used in Advanced Design System (ADS) to extract the coupling coefficient parameters.

The parameter values in Table 2.1 can then be used to calculate the efficiency of the experimental setup. At resonance, the power transfer efficiency for the two transmitter case is 10% while the single transmitter case had a 5% efficiency. The efficiency in this setup increased two fold for the multiple transmitter case and is dependent on many factors especially the distance between TX and RX. Keep in mind that having two transmitters does not guarantee a two fold increase in efficiency. These low power transfer efficiencies are primarily due to the distance between TX and RX operating in the undercoupled region. If operating in the critically coupled mode (less distance), the experimental setup can achieve up to 70% efficiency.

2.3   Effects of transmitter resonant coil coupling

The experimental setup explained in Sections 2.1 and 2.2 assume insignificant coupling between transmitter resonant coils. This assumption is acceptable since having tightly spaced transmitters reduces diversity benefits where a single interfering metal object could cause simultaneous resonant shifts at both transmitter resonant coils. Besides diversity degradation, it can be shown that there is a decreasing effect on the gain as the transmit resonant coils move closer to each other (increasing k_{24}).
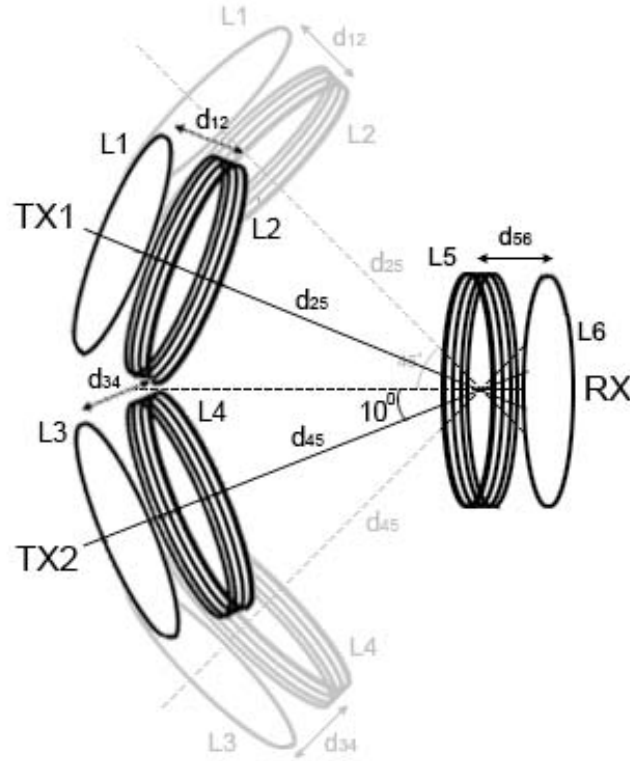
Fig. 2.8. Experimental setup for TX resonant to resonant coupling. Angle between TX and RX is reduced from 45° to 10° without changing its distance.

Simplified theoretical calculations of I_6 shown in (2.8) neglects the k_{24} coupling coefficient which signifies the amount of coupling between transmit resonant coils. To gauge the effects of having transmitter coupling, the cross coupling coefficient, k_{24}, of the resonant transmit coils is added to the impedance matrix (2.7) corresponding to Z_{24} and Z_{42}. For simplicity, similarly to (2.8), cross coupling terms are neglected with the exception of k_{24}. Fig. 2.9(a) shows the transfer function as a function of frequency and coupling coefficient k_{24}. Simulations indicate a splitting effect as the transmitter coils are brought closer to each other. The behavior of the splitting occurs differently when compared to the multiple receiver case [9] where one of the two peaks remains at the resonant frequency with the other diverging at a higher frequency. Simulation parameters were based on the values used in the previous section with a varying k_{24}
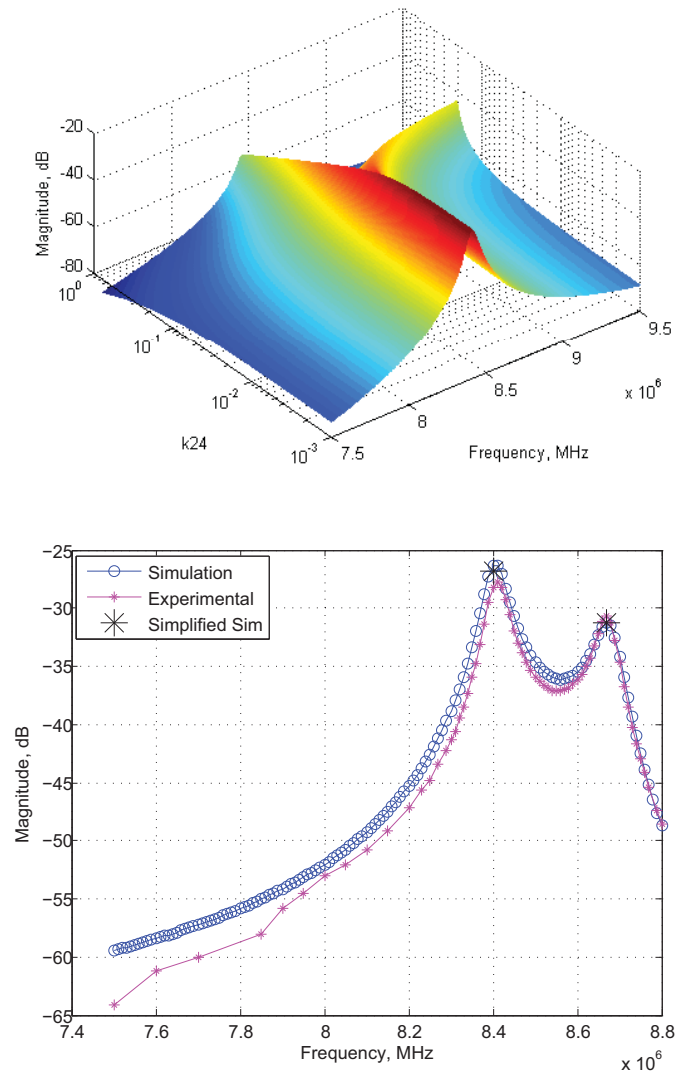
Fig. 2.9. (a) Transfer function $|V_L/V_S|$ (dB) as a function of frequency and the resonant to resonant transmit coupling coefficient k_{24} with regards to the simplified $I_{6(B)}$ equation in (2.13). (b) Simulated (complete and simplified) and measured values for the transfer function $|V_L/V_S|$ (dB) with significant resonator to resonator transmitter coupling ($k_{24} = 0.061$)

coupling term. An increase in the k_{24} coefficient represents a closer distance between TX resonant coils. Assuming the magnitude of (2.8) as

$$|I_{6(a)}| = \frac{|A|}{|B|} \tag{2.11}$$

where A is the numerator and B the denominator of (2.8) . With the addition of the k_{24} term, the magnitude of I_6 can be expressed as

$$|I_{6(b)}| = \frac{|A|}{|B + C|} \tag{2.12}$$

where $C = k_{24}\sqrt{L_2 L_4}j(-M_{12}^2 Z_{11} w^3 - Z_{11} Z_{22} Z_{66} w)$ is an added imaginary term at the denominator.

$$I_{6(b)} = \frac{jw^3 M_{12}^2 M_{25} \left(A_{S1} e^{j\theta_{S1}} + A_{S2} e^{j\theta_{S2}} \right)}{\begin{aligned} w^4 M_{12}^4 + Z_{11} Z_{66} Z_{22}^2 + w^2 Z_{11} M_{12}^2 Z_{22} + w^2 Z_{66} M_{12}^2 Z_{22} + 2w^2 Z_{11} Z_{66} M_{25}^2 \\ + M_{24} j(-M_{12}^2 Z_{11} w^3 - Z_{11} Z_{22} Z_{66} w) \end{aligned}} \tag{2.13}$$

Equation (2.13) represents the simplified equation with the added term of k_{24}. Since all the terms are non-negative, in order to maximize $|I_{6(b)}|$, the C term should approach zero ($k_{24} \to 0$). A closer look at Fig. 2.9(a) shows that as C becomes much smaller than B ($C \ll B$), the splitting peaks of the transfer function converge towards the resonant frequency and approaches the maximum value with respect to (2.8).

An experiment was conducted to see if the theoretical and simulation results would match experimental data. The setup in Fig. 2.2 was slightly modified by moving the transmitter resonant coils closer while maintaining the same distance between TX and RX as shown in Fig. 2.8. Only the angle between both TX and RX coils were minimized from $45°$ to approximately $10°$ without changing any distance between coils. Coupling coefficient values between TX and RX differ by multiplying an $\alpha = \cos(\theta)/\cos(45°)$ factor given the known $k_{(tx,rx,45°)}$ values used in Table 2.1. The following equation is used for the TX and RX coupling coefficients:

$$k_{(tx,rx,\theta)} = \alpha \ k_{(tx,rx,45°)} = \left(\frac{\cos(\theta)}{\cos(45°)} \right) k_{(tx,rx,45°)} \tag{2.11}$$

Coupling coefficients k_{12}, k_{34}, and k_{56} remain the same while transmitter to transmitter coupling coefficients k_{13}, k_{24}, k_{23} and k_{14} has values of .001, .061, .055 and .055 respectively. Table 2.2 shows the coupling coefficient values for the TX resonant to resonant coupling experiment.

Table 2.2
Coupling Coefficients for the TX-TX Coupling Experiment

Par.	Value	Par.	Value	Par.	Value
k_{12}	.2	k_{23}	.055	k_{35}	.00084
k_{13}	.001	k_{24}	.061	k_{36}	.0007
k_{14}	.055	k_{25}	.00089	k_{45}	.00089
k_{15}	.00084	k_{26}	.00084	k_{46}	.00084
k_{16}	.0007	k_{34}	.2	k_{56}	.2

Fig. 2.9(b) indicates two peaks at resonance, 8.4 MHz, and 8.67 MHz which coincides with experimental results. In theory, any increase in the k_{24} coefficient will reduce power transfer. If the A and B coefficient of the setup is operating at maximum efficiency, there is no obvious way of improving power transfer when there is significant coupling between TX resonant coils. Time multiplexing between transmitters could be implemented where one of the coil is detuned or turned off while the other is transmitting [33]. This provides similar power transfer levels as the SISO case. Transmitting with only one coil would appear to be more efficient. A 12dB difference is seen when comparing the results in Fig. 2.3 and Fig. 2.9(b). The placement of the TX coils should be at a distance such that there is insignificant interaction between TX coils but at a minimum angle orientation to increase TX and RX coupling. The optimum position for such a case for the two TX and one RX scenario is by placing all three coils in a single axis. The TX coils are placed at two opposite ends with the RX coil positioned in the middle [24]. Therefore, all coils are on the same axis at a 0° angle. Fig. 2.10 decribes the aforementioned positioning.

Tight coupling between TX only, RX only and both RX and TX result in a frequency splitting effect. Cases for different distances involving RX and TX cou-
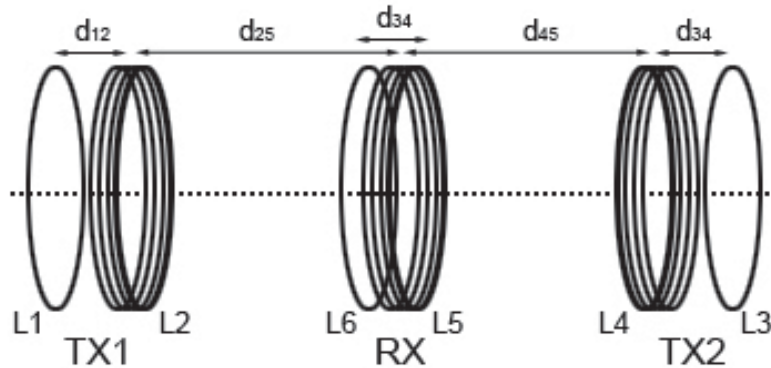
Fig. 2.10. Optimal positioning for a 2TX and 1RX experimental setup. This setup reduces coupling between transmitters while maximizing the coupling coefficient between TX and RX by having a 0° angle on the same axis.

pling have been discussed extensively with various solutions for mitigating power degradation especially for the SISO case. The received output gain through multiple transmitters as obtained in this thesis remains true for the RX and TX frequency splitting case. Fig. 2.11 shows simulations results indicating the 6dB (assuming similar characteristics of experimental setup in Fig. 2.1) for the overcoupled region, and both overcoupled together with transmitter to transmitter resonant coupling. As seen in the results, the effects of having two transmitters (6dB gain) are consistent when compared to the single transmitter case. The general framework for added gain presented is valid for both tight coupling between TX and RX and coupling between TX resonant coils. Tight coupling in the overcoupled region would result in frequency splitting and thus reduce power transfer efficiency at the intended resonance frequency.

2.4 Diversity effect of the multiple transmitter setup

Besides gain advantage, power transfer reliability is enhanced through multiple transmitters. In certain practical scenarios, foreign metal can interact with the TX
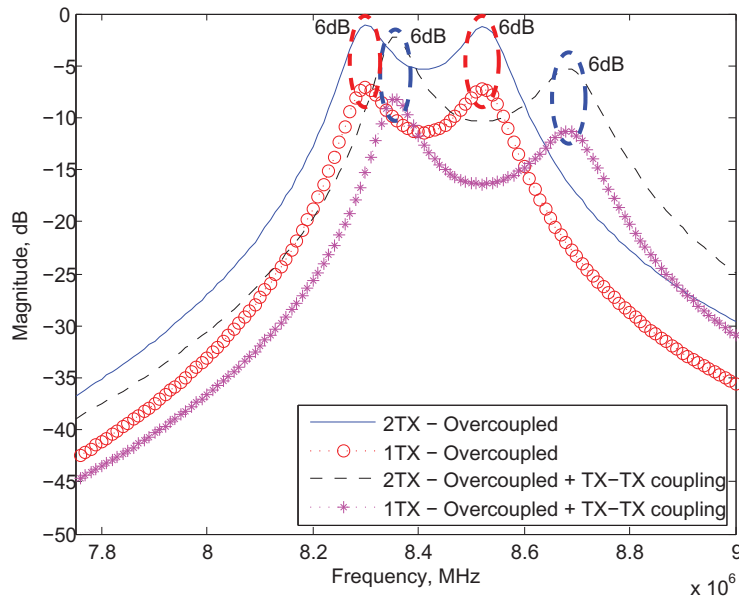
Fig. 2.11. Simulation results for the overcoupled mode (frequency splitting) including TX-TX resonant coupling for the 2TX and 1TX case. A 6dB gain is seen for the two transmitter case.

resonant coils and cause the coil's self inductance to change. A shift in resonance can cause huge power losses due to the resonant coil's high Q factor. Therefore, readjusting the resonance to the correct value is crucial. There are limitations to how much tuning can be done due to reduced magnetic flux coupling and power losses from eddy current formation.

A good conductor will allow circulating eddy currents when exposed to a changing magnetic field. This phenomenon produces an opposing magnetic field that reduces the coil's magnetic field and thus reduces its inductance. From (2.1), a decrease in inductance will result in a higher resonant frequency. The Q-factor of the resonant coil can be calculated by

$$Q = \frac{\omega L}{R} = \frac{1}{R}\sqrt{\frac{L}{C}} \tag{2.13}$$

at its resonant angular frequency $\omega = 1/\sqrt{LC}$. A decrease in the coils inductance will also result in a lower Q. To achieve acceptable power transfer efficiencies, the

lumped capacitor is readjusted to a higher value to help realign the resonant frequency. Equation (2.1) is used to estimate the retuned lumped capacitor value.
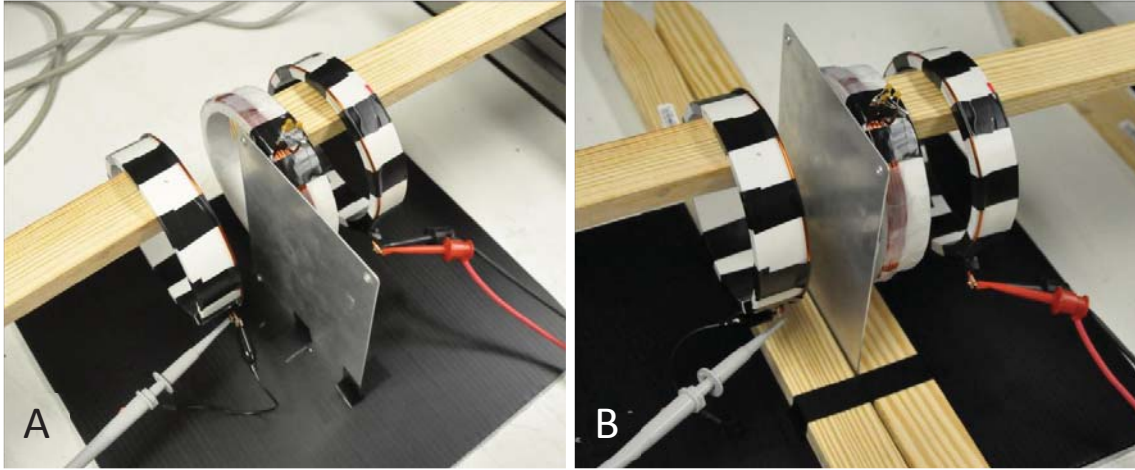
Fig. 2.12. (A) Experimental setup for the metal sheet covering half the resonant coils area. (B) Metal sheet covering a significant portion of the resonant coils area

An experiment (see Fig. 2.12) consisting of a TX pair coil and a single pick up coil receiver was conducted to understand the effects of having a metal interferer within close proximity of the resonant coil. An aluminum metal plate with dimension $17.3 \times 12.2 \times 0.1$ cm was used. The separation between each coil was 0.04 m with axes aligned. The resonant frequency and corresponding peak output voltage were observed with an oscilloscope. Fig. 2.13 shows results for three cases: 1) no plate, 2) aluminum plate covering half the coil area, and 3) covering the entire coil area.

Using the Sencore LC meter, the inductance of the coil when the metal sheet covered half and the entire area was measured at $5.35\mu H$ and $4.27\mu H$ respectively. Adjusted capacitance values of 67.1pF and 83.9pF were needed to reshift the resonance. The freespace condition had a theoretical total capacitance of 58.85pF. It is important to remember that during practical tuning of the lumped capacitor, parasitic capacitance should be taken into account.
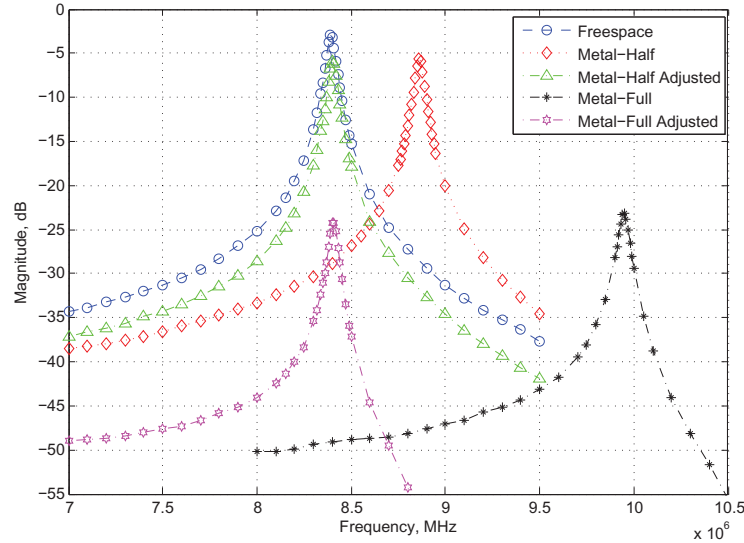
Fig. 2.13. Resonant frequency shift due to metal objects present. Two different scenarios are present where an aluminum plate is covering half the coils area and one that fully covers the area

As seen in Fig. 2.13, for the 'full metal' covering case, it is impractical to retune the resonance as there is still a significant amount of power degradation (18 dB) after resonant tuning. This is primarily due to significant reduction in the coupling coefficient between the TX and RX. One can think of the metal as a magnetic shield where the majority of the magnetic field lines flow within the metal and back to the TX coil. For the 'half metal' covered case, an initial 26dB power loss is reduced to an acceptable 2.5dB loss after retuning. In theory, if only resonance detuning occurred without loss of coupling, adjusting the capacitance value would regain original results. Multiple transmitters introduce a diversity effect that reduces the probability of outage and also maintains a certain quality of standard with regards to power transfer when compared with the SISO case.

The method of measuring and retuning the resonance is suitable for permanent internal interference such as placing coils within an electronic device containing metal content. For external type interference, detaching the system and retuning the system using an LCR analyzer is not feasible. Therefore, an automatic system to automat-

ically detect if the resonance is below or above the optimum frequency is needed. Monitoring the resonant frequency of the coil in real time is necessary and such a system for automatic capacitance tuning is subject of our ongoing research. Also, there needs to be a set threshold value for which the system should regulate or stop transmitting power due to power losses incurred at the metal object, as this will also save power consumption and reduce potential safety hazards due to unintentional heating.

2.5 Simulation results for a 2TX-1RX MISO interference scenario

The case for metal interference for the two transmitter setup in Fig. 2.1 was not experimentally performed. Simulations regarding resonance detuning were conducted for the cases explained previuosly for the two transmitter case. However, reduction of the coupling coefficient values due to eddy current formation and partial blockage of the magnetic field to the receiver were not performed. The results are shown in the figure below:
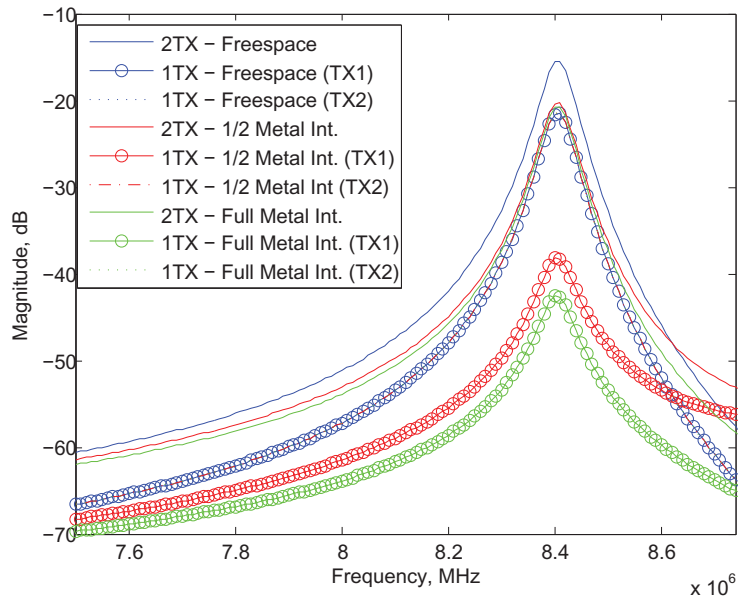
Fig. 2.14. Simulation results for the three cases (freespace, half covered metal int., full covered metal int.) with regards to the experimental parameters used in the two transmitter setup (Fig.2.1). Retuning not performed. Inductance values for the half and full interference case are $5.35\mu H$ and $4.27\mu H$ respectively.

As seen in Fig. 2.14, there is a 16.6dB reduction in the half covered case while the full covered case had a reduction of 20.98dB. The metal interference was simulated on TX1 while TX2 was without any interference. The combined received transfer function value at the receiver behaves almost as if only TX2 was transmitting since the additional gain due to TX1 is minimal. Fig. 2.15 shows simulation results with retuned capacitance values to get the correct resonance frequency of 8.4MHz. With proper tuning, if there is no coupling coefficient (k_{25}) reduction (which is not feasible in real life due to eddy current formation and a partially shielded magnetic field which lowers the coupling coefficient), theoretically the system performs as well as the freespace case. An algorithm for an automatic retuning process is needed and is subject of our future work.
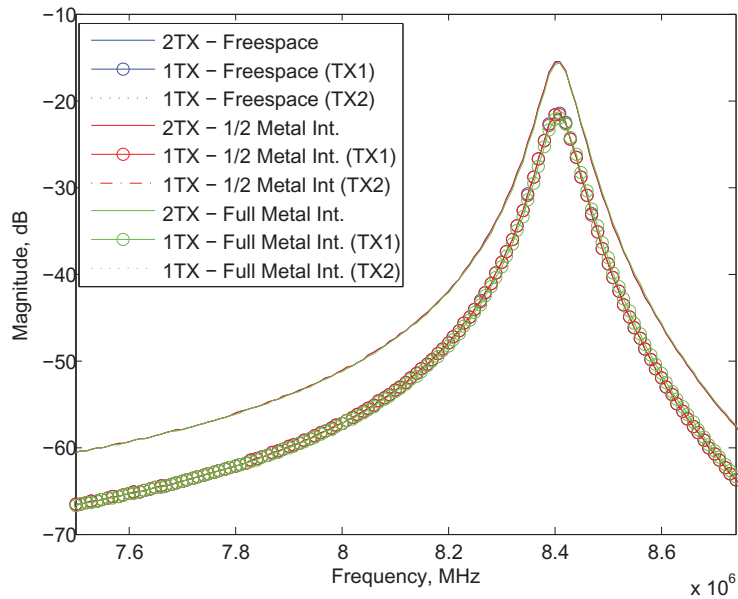
Fig. 2.15. Simulation results for the three cases (freespace, half covered metal int., full covered metal int.) with regards to the experimental parameters used in the two transmitter setup (Fig. 2.1). Retuning of the capacitors for the correct resonance was performed. Adjusted capacitance value for the half and full interference case is 67.1pF and 83.9pF respectively.

2.6 Practical implementation for the multiple transmitter setup via power line

The multiple transmitter experiment conducted in chapter II used a dedicated wire to establish synchronization. One unique way of synchronizing the driving signals is to utilize the power line infrastructure. This reduces the need of additional wiring or an RF front end module. Another useful reason for utilizing the power line network is the flexibility of sending different driving frequencies if automatic frequency tuning is needed in case of frequency splitting in the overcoupled region [16].

Power lines were built primarily for power transmission and were not optimized for efficient wireline communications. Some of the issues associated with PLC communications include impedance mismatch, absence of EMI shielding and the existence of
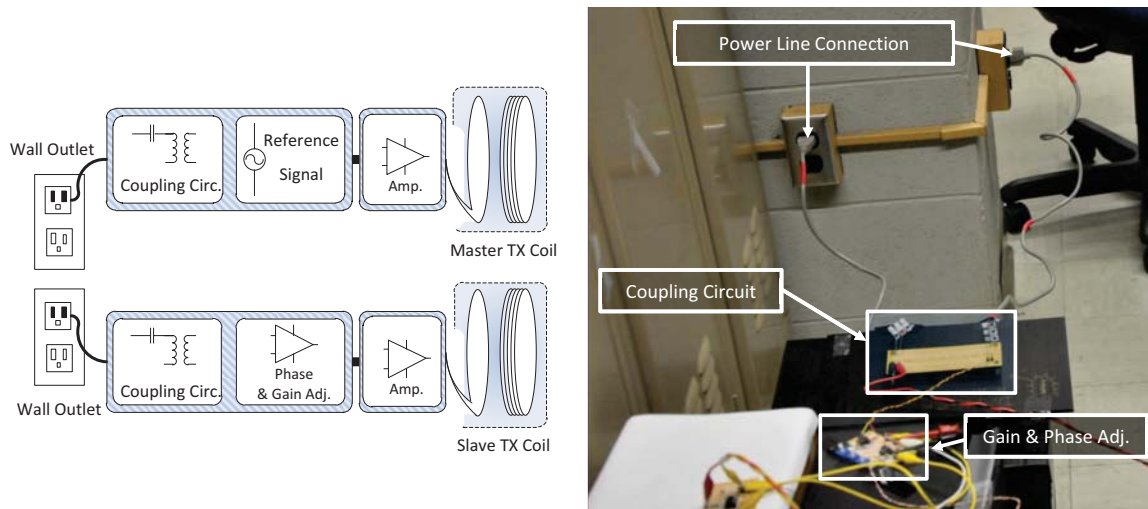
Fig. 2.16. (A) Block Diagram, (B) Picture of the power line communication synchronization technique for multiple transmitter wireless power transfer via coupled magnetic resonance.

detrimental noise sources varying with both frequency and time. The main objective of this experiment is to use the already available infrastructure to send a reference signal in order to synchronize the magnetic field transmitted from both transmit coils. The overall setup for the PLC synchronization technique is shown in Fig. 2.16.

2.7 Coupling circuit & gain and phase adjustment

A coupling circuit is needed to block the power line's 120 V$_{rms}$ 60 Hz sinusoidal signal and to inject the intended driving signal of 8.4 MHz. A high pass filter with a reasonable cutoff frequency was used as a medium to channel signals through the power line network. A high voltage capacitor valued at 100 pF, 1000 V rating together with a 1:1 high frequency transformer (CoilCraft, PWB-1-AL, 0.08–450 MHz Bandwidth) with an inductance of 40 μH was utilized to pass signals above 2.5 MHz. The high pass filter was configured as an LC filter. See Fig. 2.18. This circuit configuration is known as a transformer-capacitor coupler design and is used in many

PLC products. The advantage of using a transformer is due to its ability to provide galvanic isolation, impedance matching, and also to act as a limiter in case of high voltage transients [28].
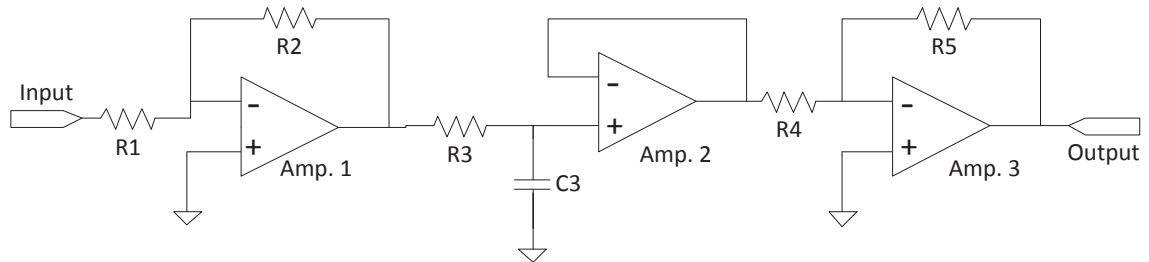
Fig. 2.17. Gain and phase adjustment circuit diagram.
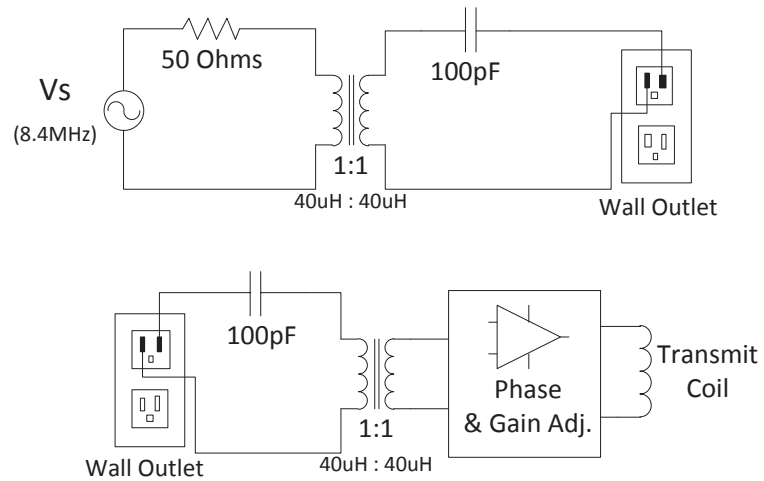
Fig. 2.18. Coupling circuit diagram connecting the reference signal (8.4MHz) to the slave transmit coil via power line communications.

Due to the frequency response of the coupling circuit and the power line itself, the signal transmitted will have distortion in terms of both magnitude and phase. Therefore, a gain and phase adjustment circuit was needed (Fig. 2.17). An LM6171BIN National Semiconductor amplifier with unity gain bandwidth of 100 MHz was used

to drive the power transmitter coils with an external 50 Ω resistor in series with the output. This particular amplifier was used for theoretical purposes due to the flexibility of modifying or modulating specific signals for future research and is not capable of handling high output current. If higher power is needed, a class-E amplifier setup can be used [32].

The reference signal after traversing the coupling circuit and power line has a peak to peak voltage of 674 mV, a reduction of 17.4 dB from its original 5 V peak-to-peak value. In addition, there is a phase difference of 49° corresponding to 16.3 nsec of delay. The design of the gain and phase adjustment circuit is given in the equations below. For phase adjustment, ideally, the values for components R_3 and C_3 as in Fig. 2.17 can be chosen using the transfer function of the basic RC setup

$$H_{RC} = \frac{V_{out}}{V_{in}} = \frac{1/(j\omega C_3)}{1/(j\omega C_3) + R_3} = \frac{1 - j\omega R_3 C_3}{1 + \omega^2 R_3^2 C_3^2} \tag{2.14}$$

with the magnitude and phase to be

$$|H_{RC}| = 1/\sqrt{1 + \omega^2 R_3^2 C_3^2} \tag{2.15}$$

$$\angle H_{RC} = \tan^{-1}(-\omega R_3 C_3) \tag{2.16}$$

Values $R_3 = 11.01$ kΩ and $C_3 = 2$ pF provides the necessary phase shift of approximately $\angle H_{RC} = 310.7°$ but causes a decrease in magnitude of $|H_{RC}| = 0.6522$ or -3.71 dB. The total gain, G, of 21.11 dB is now needed to increase the Vpp from 440mV to 5V. Each inverting amplifier 1 and 3 in Fig. 2.17 has a gain , $G_1 = -R_2/R_1$ and $G_3 = -R_5/R_4$, where the total gain is the multiplication of G_1 and G_3. Gains, G_1 and G_3 can be set arbitrarily as long as the total gain equals 11.36 or 21.11 dB. Experimentally, instead of using fixed resistors, variable resistors R_2, R_3, and R_5 were used to manually tweak the gain and phase. This is due to the amplifier's internal delay which also varies according to the gain setting. Fig. 2.19(B) shows the corrected reference signal for the slave transmitter coil. Only a slight phase offset of 5° is seen after phase and gain tweaking.
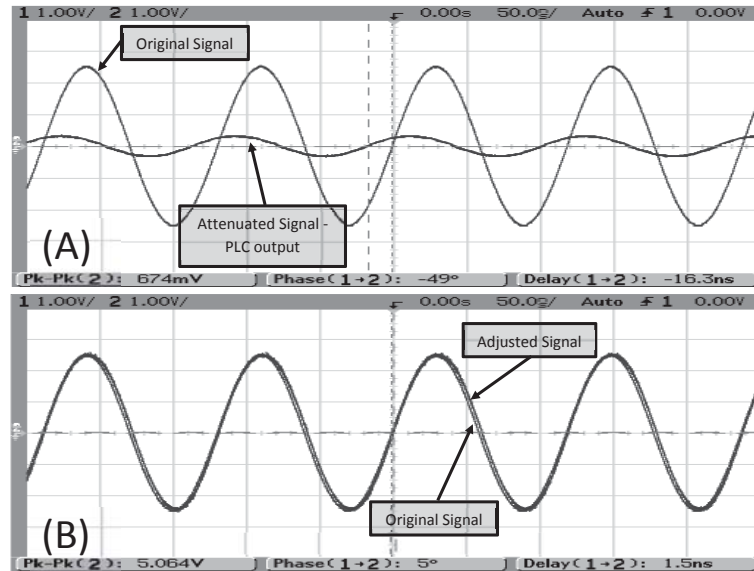
Fig. 2.19. (A) 8.4MHz reference signal before phase and gain adjustment. (B) after gain and phase adjustment.

If the positions of the transmitters are static with a relatively stable power line channel condition, manually tweaking the gain and phase of the synchronization signal would suffice. For a more dynamic solution with varying transmitter positions, an automatic gain and phase tuning system would be more practical. This automatic solution could incorporate a feedback channel between receiver and transmitter to automatically adjust its driving signal at the slave transmitter for optimum power transfer. Communications through the magnetic field itself, for example, an RFID type communication system could be implemented. If a low frequency driving signal is used, for example the Qi wireless power standard frequency range (100kHz - 200kHz), phase delays become inconsequential. This reduces the need of an automatic adjustment system and synchronization through PLC proves to be a very simple method when compared to a wireless solution.
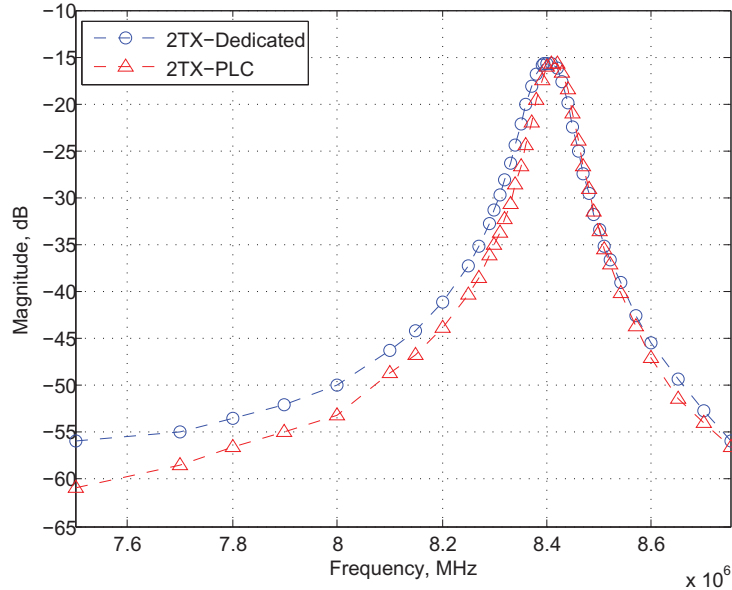
Fig. 2.20. Transfer Function $|V_L/V_s|$ (dB) for experimental measurements for dedicated and PLC synchronization techniques.

2.7.1 Experimental results

Fig. 2.20 shows the measured transfer function of the multiple transmitter setup using the power line communication synchronization technique together with the dedicated wire technique. The phase and gain adjustment was tuned to work specifically at 8.4 MHz resonant frequency. The frequency response of the power line channel could vary in both magnitude and phase at different frequencies. However, for this experimental setup, it is acceptable since the wireless power transfer system is designed to work at resonance. At 8.4 MHz specifically, the transfer function of the PLC synchronization technique performs equally with the dedicated wire technique.

2.8 Conclusion

A multiple transmitter wireless power transfer scheme via coupled magnetic resonance is analyzed using electrical circuit theory. For the case of two multiple transmit coils, the gain and diversity effect is presented. Negative effect of transmitter resonant

coupling is shown theoretically and experimentally. Practical synchronization issues with regard to frequency and phase is presented for the multiple transmitter case. Experiments were also conducted to gauge the effect of resonant frequency shifting due to nearby metallic objects. Frequency shifts can be readjusted to the correct frequency by performing capacitance tuning. A practical synchronization technique is presented to ensure proper magnetic field combining at the receiver coil. This was done via power line communications with appropriate gain and phase tuning.

3. TIME DIVISION MULTIPLEXING (TDM) FOR TIGHTLY COUPLED RECEIVERS

3.1 An Introduction to Multiple Receivers

Multiple receivers in a CMR-type wireless power system can be thought as multiple users, each with his own receive coil pair. Multiple receive resonant coils are not used within the same user due to coupling and the physical limit of the coil size. Mobile devices are generally portable and the area size of the coil is preferred to be as large as possible to maximize the RX-TX coupling coefficient. This is assuming a sizeable transmitter for a wide area of charging.

As an introduction, an ideal general N-receiver and single transmitter setup with negligible coupling between receivers is used to show how received power scales according to the number of N receivers. Using the circuit theory method explained in Chapter 2, the general current equation for equivalent loads is given by

$$I_{L_N} = \frac{jw^3 M_{12}^2 M_{23} V_S}{w^4 M_{12}^4 + 2M_{12}^2 Z_L Z_R w^2 + \mathbf{N} M_{23}^2 Z_L^2 w^2 + Z_L^2 Z_R^2}. \tag{3.1}$$

M_{12} is the mutual inductance between the source/load and resonant coils while M_{23} represents the mutual inductance between the transmitter and receiver resonant coils. The TX source coil impedance Z_S and all the receivers load coil impedance Z_L are assumed to be identical resulting in

$$Z_L = Z_S = R_L + R_N + jwL_N = R_S + R_{TX} + jwL_{TX}. \tag{3.2}$$

R_S is the output resistance of the TX and R_L is the load resistance value. For simplicity in writing (3.1), the parameters are kept to be equal including the AC resistances R_N and R_{TX} and the source and load coil's inductance values of L_N and

L_{TX}. The resonant coil impedance value for the transmitter and all N receivers is given by

$$Z_R = jwL_R + \frac{1}{jwC_R} + R_R. \tag{3.3}$$
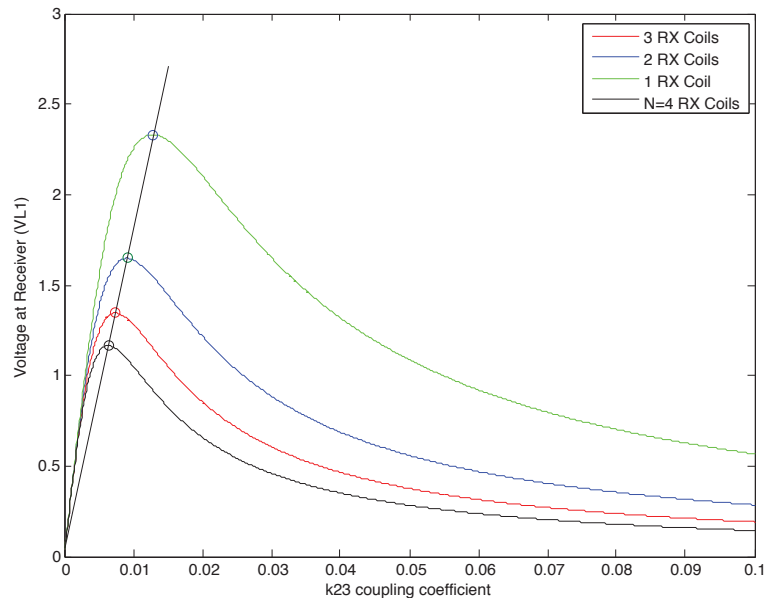
Fig. 3.1. Simulated received voltage with N received coils with varying k_{23} values. (N ranging from 1 to 4)

Fig. 3.1 shows the received voltage with varying RX-TX coupling (k_{23}). k_{23} is the coupling coefficient between the transmitter's resonant coil and the receiver's resonant coil. It is primarily related to the distance between TX and RX. It can be seen that maximum voltage for different N receivers occurs at different distances. If more receivers are added, the distance between RX and TX should be increased to produce maximum received power. A straight line across the maximum points (see Fig. 3.1) for each N receivers can be drawn and one can predict the amount of distance needed for maximum power transfer for N receivers. Another important point on the significance of this line is the region of operation whether one is operating in the critical, overcoupled or undercoupled region. Points at the line itself are the critically coupled point while points on the right show an overcoupled region and to

the left of the line is the undercoupled region. The simulations for N=1,2 and 3 were simulated using actual simplified impedance matrices.

If receivers are added, changing the distance for optimum power is impractical and receivers are typically placed at the same distance with regards to the SISO case. The distance placed for the single receiver case turns into the overcoupled region where added receivers experience frequency splitting. One solution to this problem is by varying the k_{12} coupling coefficient between the driver/load coil and its corresponding resonant coil [17] . The adjustment of k_{12} provides a matching condition by repositioning the system into the critically coupled state. Table 3.1 shows the received power or voltage information and its power degradation percentage if operated at the same distance (with regards to the SISO case).

Table 3.1

1xN TX-RX - Received voltage at different k_{23} values. $(k_{12} = 0.2, \forall N)$

N	k_{23}	V	k_{23}	Max V	% Voltage Degradation
1	.0129	2.33	.0129	2.33	0%
2	.0129	1.54	.0091	1.648	12.68%
3	.0129	1.15	.0074	1.346	27.0 %
4	.0129	.9157	.0053	1.165	38.22%

As indicated in Table 3.2, adding receivers with the same distance to the SISO case significantly degrades performance. In a practical case, receivers would tend to be placed near each other and this implies close proximity and equidistance from all the receivers to the transmitter. As an introduction, non-coupling receivers are discussed while multiple receiver coupling is discussed in the upcoming chapters. Fig. 3.2 shows the system adapting to receivers being added and an initial solution on how the k_{12} coupling coefficient can be adjusted to achieve optimal power transmission.

When taking a closer look at Fig. 3.1, if reduced efficiency can be tolerated, one can operate at further distances with a k_{12} value of less than 0.0337. At this distance, a system with up to 4 receivers will be able to achieve equal received power without
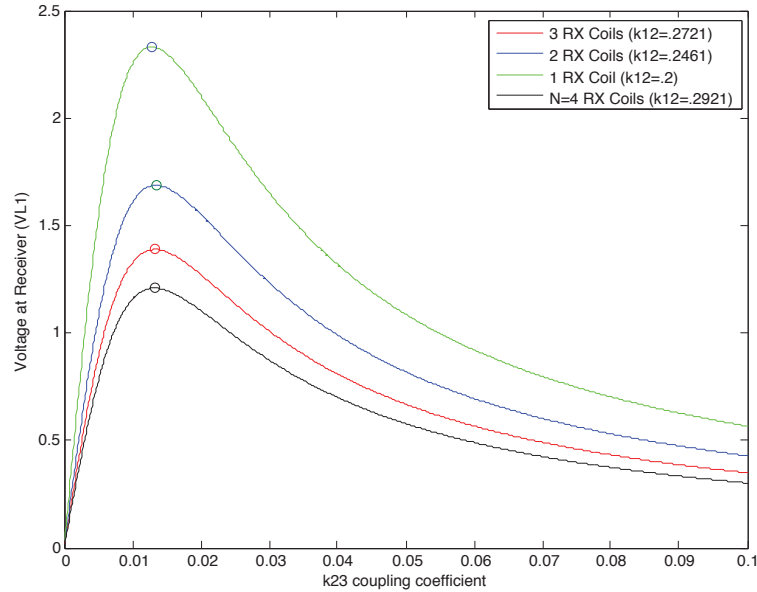
Fig. 3.2. Simulated received voltage with N received coils with varying k_{23} values. k_{12} adjusted for optimum power transfer at $k_{23} = 0.0129$

any changes in the system. Operating at loose TX-RX coupling values allows the flexibility of additional receivers and added additional distance but reduces efficiency when only small numbers of receivers are being powered. The TDM method proposed in the next section eliminates the need for matching or k_{12} coupling adjustments and is intended to be used when receivers are placed close to each other.

3.2 TDM and the Multiple Receiver System Overview

3.2.1 The Multiple Coil Receiver Setup

Multiple receivers for a WPT system can be viewed as a multi-user scenario where each receiver has only one pair of resonant and load coils. Having multiple receiver coils on each unit degrades performance by introducing coupling effects within the system and reduces the geometric size of the coils. The signal processing needed for multicoil powering has a close relationship to the techniques used in multiuser communication. In an ideal case where coupling between receivers can be ignored,

N users can be charged simultaneously by a single transmitter with the total power divided equally. This reduces cost and clutter by eliminating the use of power cables. To demonstrate our approach, the two receive coil scenario is considered.

Fig. 3.3 shows the two receiver and single transmitter setup. The phasor current
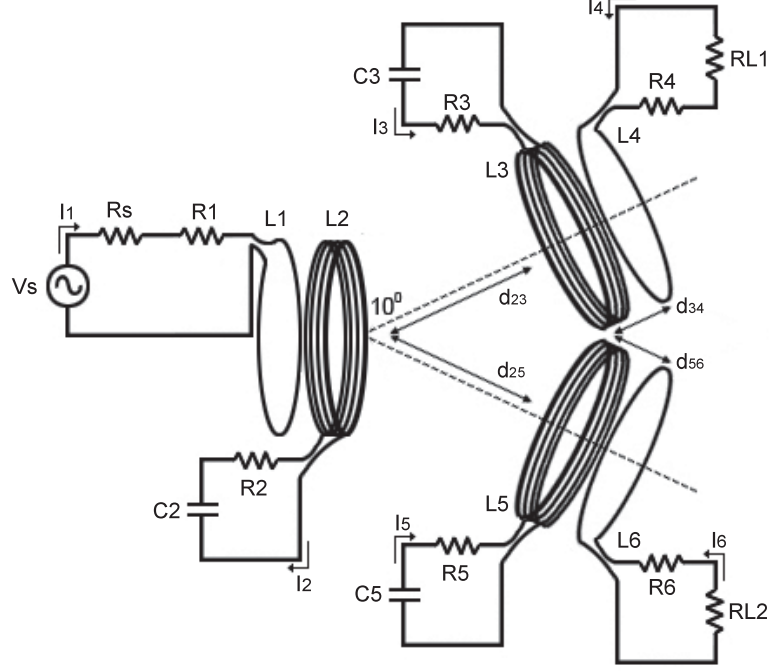
Fig. 3.3. A one transmitter and two receiver experimental setup with close RX-RX coupling

can be calculated at each coil loop according to

$$
\begin{bmatrix} I_1 \\ I_2 \\ I_3 \\ I_4 \\ I_5 \\ I_6 \end{bmatrix} = \left[\{Z_{k,\ell}\}_{1 \leq k,\ell \leq 6} \right]^{-1} \begin{bmatrix} V_S \\ 0 \\ 0 \\ 0 \\ 0 \\ 0 \end{bmatrix} \tag{3.4}
$$

with individual impedances ($Z_{k,\ell}$) given by

$$Z_{11} = j\omega L_1 + R_S + R_1$$

$$Z_{22} = j\omega L_2 + R_2 + \frac{1}{j\omega C_2}$$

$$Z_{33} = j\omega L_3 + R_3 + \frac{1}{j\omega C_3}$$

$$Z_{44} = j\omega L_4 + R_4 + R_{L1}$$

$$Z_{55} = j\omega L_5 + R_5 + \frac{1}{j\omega C_5}$$

$$Z_{66} = j\omega L_6 + R_6 + R_{L2}$$

$$Z_{k,\ell} = Z_{\ell,k} = \pm j\omega M_{k,\ell} , \ k \neq \ell \tag{3.5}$$

I_k with $k = \{1, \ldots, 6\}$ represents the individual received phasor current at coil k. $Z_{k,\ell}$ is the corresponding impedance interaction for coils k and ℓ with $Z_{\ell,k} = Z_{k,\ell}$. V_S denotes the transmitter phasor voltage. L_k is the k-th coil's inductance value with R_k representing the AC resistance for coil k. R_S is the TX source resistance with R_{L1} and R_{L2} representing the load values for RX_1 and RX_2. I_4 and I_6 in (3.4) represent the phasor current at each RX load. For simplicity, a loose coupling case is assumed where cross coupling factors between RX-TX and RX-RX are set to zero. This assumption provides mathematical insight as to how tight RX resonant coupling affects the load current. The load current equation becomes very complex if all coupling coefficients are taken into account. Fortunately, as will be shown in Section 3.5, experimental and simplified simulation results only differ slightly with regards to its transfer function magnitude at resonant peaks.

The **Z**-impedance matrix given by

$$\mathbf{Z} = \begin{bmatrix} Z_S & jwM_{12} & 0 & 0 & 0 & 0 \\ jwM_{12} & Z_R & jwM_{23} & 0 & jwM_{23} & 0 \\ 0 & jwM_{23} & Z_R & jwM_{12} & -jwM_{35} & 0 \\ 0 & 0 & jwM_{12} & Z_L & 0 & 0 \\ 0 & jwM_{23} & -jwM_{35} & 0 & Z_R & jwM_{12} \\ 0 & 0 & 0 & 0 & jwM_{12} & Z_L \end{bmatrix} \tag{3.3}$$

is used in (3.4) to form a simplified receiver current equation in I_4 and I_6 as shown by

$$I_4 = I_6 = \frac{jw^3 M_{12}^2 M_{23}\ V_S}{\begin{aligned}w^4 M_{12}^4 + Z_S Z_R^2 Z_L + w^2 Z_S Z_R M_{12}^2 + w^2 Z_R Z_L M_{12}^2 + (2)w^2 Z_S Z_L M_{23}^2 \\ + \underbrace{jM_{35}(-M_{12}^2 Z_L w^3 - Z_S Z_R Z_L w)}_{\text{x}}\end{aligned}}.$$

$$(3.4)$$

The distance between receivers to the transmitter is assumed to be equal for simplicity. The assumption is that the distance of tightly coupled receivers have similar distances to the transmitter. Since the resonant coils and load coils are similarly designed, the impedance component of Z_{22}, Z_{33} and Z_{55} are represented with one variable, Z_R. Also, Z_{66} is equal to Z_{44} assuming equal load resistances and is represented as Z_L. Z_{11} is termed as Z_S. The coupling coefficient between the driving/load coil to the resonant coil is represented with the impedance component of jwM_{12} while coupling between TX and RX is represented with the jwM_{23} component. jwM_{35} represents RX-RX resonant coil coupling.

The **Z**-impedance matrix can be used to quickly view which coil interaction is being taken into account for calculating received current in the simplified condition. The voltage received at R_{L1} and R_{L2} are $V_{L1} = |I_4 R_{L1}|$ and $V_{L2} = |I_6 R_{L2}|$, respectively. Solving (3.4) by inserting (3.3), I_4 and I_6 can be represented in a simplified equation as seen in (3.4). It represents a one TX by two RX setup with RX-RX coupling.

3.2.2 Frequency Splitting for Tightly Coupled Receivers

Charging multiple coils simultaneously can be challenging due to the interaction between the coils through the phenomenon of frequency splitting. At a high level, frequency splitting can be thought of a shift in the effective resonant frequency due to interaction between the receive coils. In a multiple receiver case, frequency splitting due to receiver coupling was first shown in [9]. The effect of RX-RX coupling can be

shown theoretically through the simplified equation in (3.4), where the **x** term given by

$$\mathbf{x} = jM_{35}(-M_{12}^2 Z_L w^3 - Z_S Z_R Z_L w) \tag{3.5}$$

becomes significantly large as the mutual inductance M_{35} increases due to a higher value of k_{35}. The coupling coefficient is related to the mutual inductance as shown by

$$M_{x,y} = M_{y,x} = k_{x,y}\sqrt{L_x L_y}. \tag{3.6}$$

The **x** term (3.14) grows large as the receivers are brought closer to each other and starts to significantly affect the received current due to its presence in (3.4). This is not obvious in the resonant-inductive method because the coupling term between receivers is small enough to not affect the overall transfer function unlike the CMR case. Intuitively, one can think of the CMR-type resonant coil of having much higher currents that extend the induced magnetic field due to its low impedance at resonance. This is one of the main reasons why it achieves longer distances at low TX and RX coupling coefficients when compared to an inductive or resonant-inductive scheme. A significant **x** term value in (3.4) creates the splitting effect due to its resonant properties. The term is a complex value with similar magnitude resonant characteristics but at different phase values in frequency.

In the experimental setup, the distance between RX and TX is set such that it exceeds the overcoupling region [16] to avoid RX-TX frequency splitting. It is important to note that depending on the resonant coil coupling (RX-TX, TX-TX or RX-RX), the transfer function will exhibit resonant peaks at two different frequencies. For TX-TX and RX-RX resonant coil coupling, one peak is situated at the resonant frequency and the other peak occurs at a higher frequency. RX-TX frequency splitting has each peak diverging away from the resonant frequency. The impedance seen by the transmitter is altered when frequency splitting occurs.
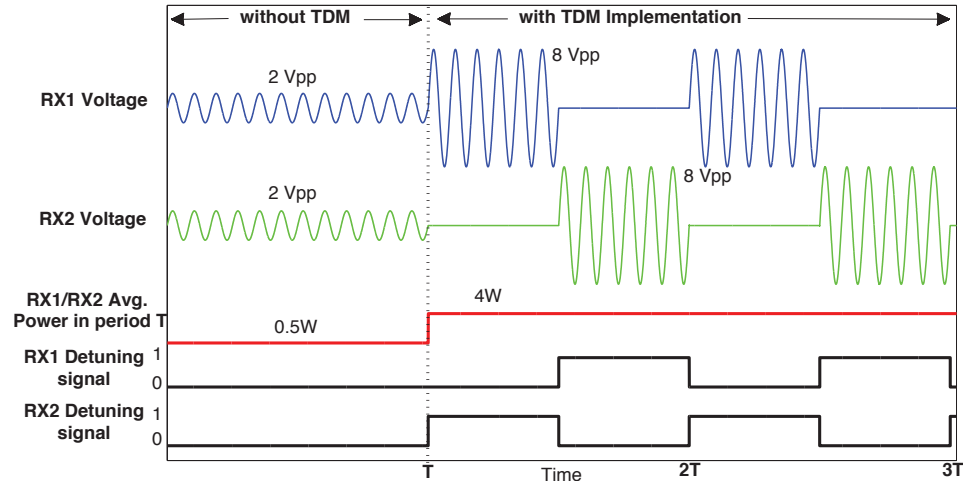
Fig. 3.4. An illustration on how TDM can improve the total average received power. This example assumes two receivers in a tightly coupled scenario where they are placed very close to each other. RX_1 and RX_2 share the same average received power over period T. In this example, the received power is eight times the power received in the non-TDM mode.

3.2.3 The Time Division Multiplexing Scheme

Time division multiplexing is a concept commonly used in communications to send and receive data through a shared channel. There is interference between multiple users if data is sent simultaneously within the same channel and to avoid this, each user can be served individually using non-overlapping time slots. The TDM technique for wireless power transfer has a similar analogy where closely coupled receivers add 'interference' within the WPT system. If the interfering resonant coil is detuned, the received signal can be significantly increased. Fig. 3.4 gives a brief introduction on the idea and benefits of TDM implementation for a two receiver case. Each receiver will detune its resonant coil at a specific time slot per the transmitter's instruction.

In the example shown in Fig. 3.4, the receivers detune 50% of the time. Even though both are powered for half the time, the total average power over time is significantly higher when compared to a system without TDM. The improvement depends on how tight the coupling is between receivers.

The TDM periodic cycle time starts from time $t = 0$ to $t = \sum_{j=0}^{N} T_j$ and can be represented as $[T_0 , \sum_{j=0}^{N} T_j]$. T_0 is defined to be equal to zero. T_j can be viewed as the charging duration for the j-th receiver while N is the total number of receivers present. The unique time slot for the i-th receiver can be written as $[\sum_{j=0}^{i-1} T_j , \sum_{j=0}^{i} T_j]$. For example, RX_1 will have its specific allocation time of $[0, T_1]$ with RX_2 having a $[T_1, T_1 + T_2]$ time slot. A generalized received power equation for user i can be expressed as

$$P_{RX,i} = \frac{\sum_{j=0}^{i} T_j - \sum_{j=0}^{i-1} T_j}{\sum_{j=0}^{N} T_j} (P_{TX}) \tag{3.7}$$

where P_{TX} is the total allocated power. If equal power distribution is used, (3.7) can be further simplified as

$$P_{RX,equal} = \frac{T_j P_{TX}}{N T_j} = \frac{P_{TX}}{N}. \tag{3.8}$$

3.3   TDM proof-of-concept through ADS simulation

For a two coil receiver system with very tight coupling, detuning one of the receivers and transmitting power to only one receiver could provide better transmitted power. A predetermined coupling coefficient (k_{rx}) threshold value is needed to initiate time multiplexing. There comes a point where powering the coil individually would produce higher overall received power if multiple receiver coupling becomes too detrimental. The basic idea is to completely detune one of the two receivers and operate in SISO mode within a certain time slot. The received voltage V_{load} for a SIMO case with minute RX-RX coupling and tight coupling is shown in Figs. 3.5 and 3.6 using Advanced Design System (ADS). ADS is used to simulate the SIMO system in frequency and time domain for cases involving loose and tight coupling situations. The time division multiplexing solution is also shown in ADS and is presented in time domain as seen in Fig. 3.7.

The distance between TX and RX is fixed to be equal, hence V_{load} at both Receivers 1 and 2 are equal. Since the results are the same, we only show the received voltage
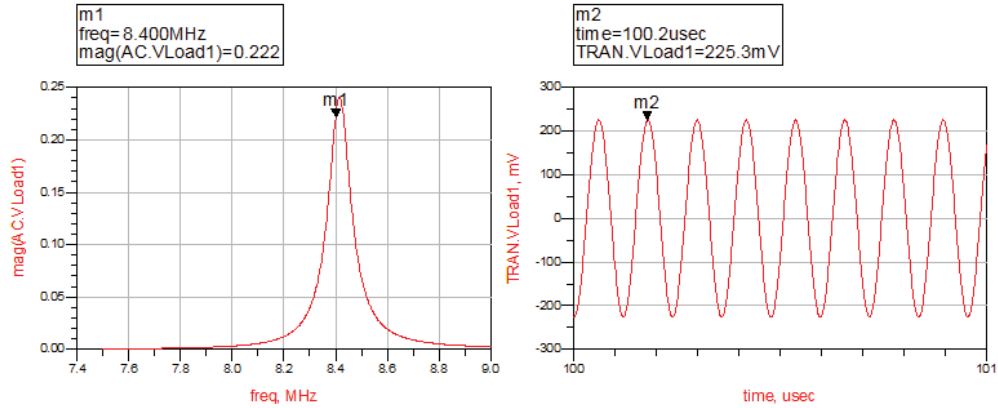
Fig. 3.5. Voltage load (V_{load}) at Receiver 1 for a 1 x 2 SIMO system without RX-RX coupling in frequency and time domain.
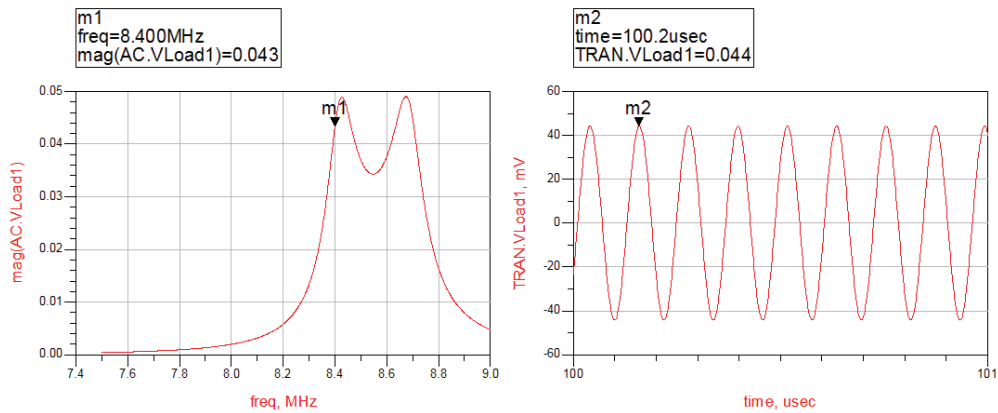
Fig. 3.6. Voltage load (V_{load}) at Receiver 1 for a 1 x 2 SIMO system with significant RX-RX coupling in frequency and time domain.

at Receiver 1. Fig. 3.5 has a maximum received peak voltage of 222mV. This setup assumes loose coupling between both TX-RX and RX-RX with a coupling coefficient of k_{23} and k_{25} of 0.00064 and k_{35} of zero. Fig. 3.6 then shows what happens when significant coupling ($k_{35} = 0.061$) is seen between receivers. The voltage received at Receiver 1 is reduced significantly with a value of 43mV. This constitutes an 80% voltage reduction or a staggering 96% power reduction. Essentially, the whole system breaks down once receivers come close together. Magnetic resonance coupling brings
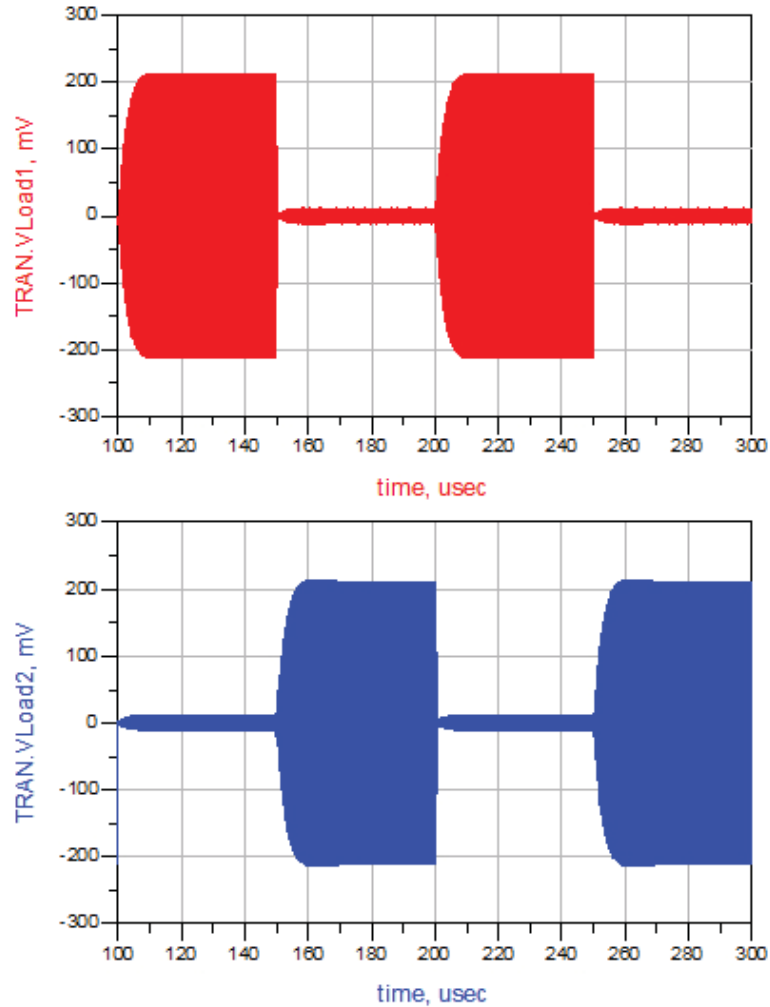
Fig. 3.7. Voltage load (V_{load}) at Receiver 1 for a 1 x 2 SIMO system implementing time division multiplexing with significant RX-RX coupling (results in time domain).

great advantages in increasing distance with high efficiency but is highly susceptible to nearby equivalent resonators.

A time division multiplexing technique as seen in communications can be used to effectively detune one resonator at a time and operate in SISO mode. Basically, the receiver which is not being charged/powered is invisible to the receiving load. Hence, the receiver will receive full power in accordance to a 1 x 1 system but only at its designated slot time. For equal powering times with a 1 x 2 SIMO system, a

50% duty cycle between Receivers 1 and 2 can be used. The switching times can be varied corresponding to different charge states at the receivers. If one receiver has full charge, 100% of the switching time can be used by the other receiver. A scheme to intelligently detune the resonators with synchronized on and off times is needed in practice. As of now, we can show this result theoretically through ADS simulations. Receiving full power for half the amount of time is still more beneficial than having a continuous 96% degraded received power.

The TDM solution results in a peak received voltage of around 212mV shown in Fig. 3.7. The on and off times are synchronized using a common squarewave signal with a frequency of 10kHz. This gives an on and off time of $50\mu s$ for each receiver. For our simulation setup, the received average power at each receiver can be calculated by

$$P_{ave} = \left(\frac{1}{2}\right) \frac{V_{RMS}^2}{R_L} \tag{3.9}$$

for a 50% on/off time. The average power received at each load is then 50% of the SISO case for the loose coupling case. We compare the results for the RX-RX receiver coupling with and without the implemented TDM solution. Table 3.2 shows the received power results for the three cases.

Table 3.2
Received power in mW and percentages for the three cases involving
RX-RX coupling.

Case	V_{load} (mV)	$P_{ave,}$ (mW)	% Difference
1x2 or 1x1 No RX-RX coupling	222	0.493	0%
1x2 RX-RX coupling no TDM	43	0.0185	96%
1x2 RX-RX coupling with TDM	212 (50%)	0.225	54.4%

The received power for the RX-RX coupling case with the TDM solution has roughly 13 times more received power when compared to the non-TDM case. The results shown in Table 3.2 assume loose coupling between the transmitter and receiver (large transfer distances). This is why the voltage received for the 1x1 and 1x2 case is

nearly the same as seen on the left portion of the straight line in Fig. 3.1. It was shown earlier that if operated at the critically coupled range for the SISO case, the received voltage is higher when compared to the two receiver case without significant RX-RX coupling. The advantages of TDM are enhanced further if the RX-TX distance is closer. Another important benefit of using TDM is that even though half the average power is transferred, the voltage level transferred is maximized to perform DC rectification. If a suitable synchronization frequency is chosen, the DC output of the full bridge rectifier can be made smooth with a carefully chosen capacitor value.

Fig. 3.8 is the overall SIMO system circuit diagram simulated in ADS. Experimental data is is discussed further in Section 3.5.2.
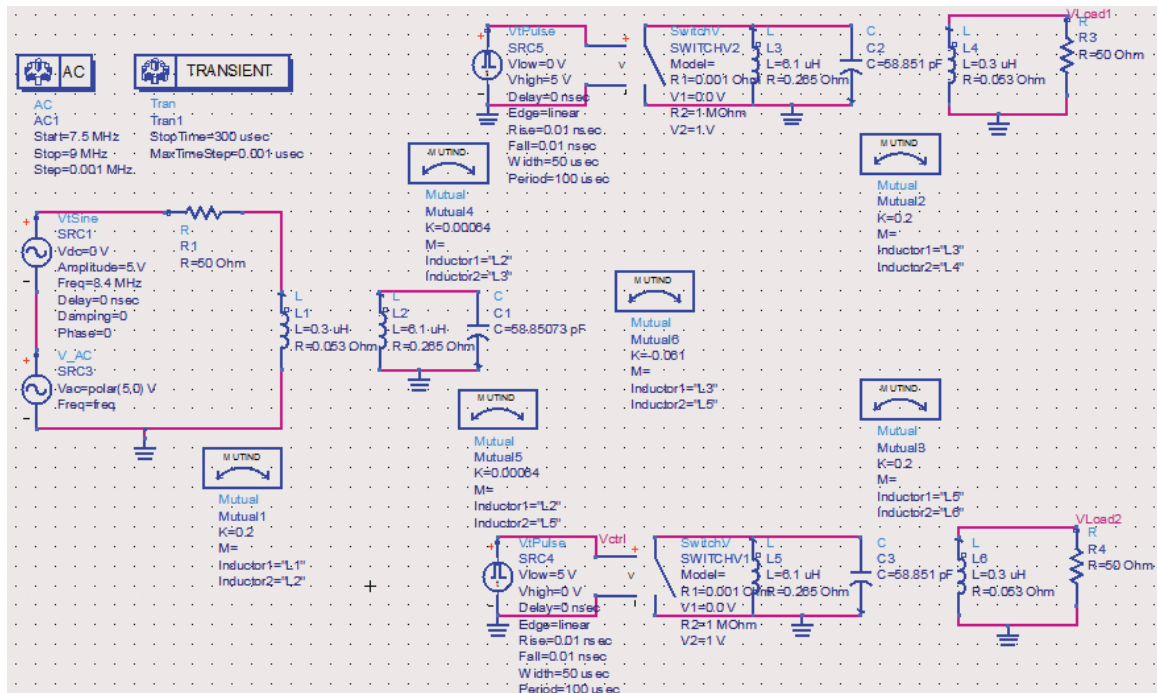
Fig. 3.8. ADS schematic diagram used for loose, tight and time division multiplexing simulation of the 1x2 SIMO system.

Proper synchronization among the receivers is needed to turn on at specific time slots. Ideas range from a synchronized timing clock which is available to all receivers

to indicate when their specific turn on/off time is. The downside of time multiplexing is that the amount of power transferred approaches zero as the number of receivers increase to infinity. This is primarily due to the charge/power on time because only one coil can be turned on at the same time.

If the location or coupling coefficient between receivers could be accurately determined, an increase in the number of receivers could be obtained by simultaneously powering loosely coupled receivers. For example, in a three receiver case, where they are lined up in a row, only the middle coil would be tightly coupled with its left and right coils. This enables slightly loose coupling between the left and right coils and both coils could be powered on with only the middle receiver detuned. An illustration is shown in Fig. 3.19 and is explained further in Section 3.6.1.

3.4 TDM Circuit Implementation for Detuning and Synchronizing

Tight coupling between resonant RX receivers will result in a reduction of induced current at both resonant coils. Interactions between RX resonant coils being induced from a single synchronized source will produce opposing magnetic fields between each other. This occurs regardless of the coil's winding direction as the TX field seen is identical. The direction of current flow in the circuitry is a function of the coil's winding but not its opposing magnetic field produced from each RX resonator coil i.e., Lenz's Law.

The basic principle behind implementing CMR is to increase magnetic flux or current at the TX and RX resonant coil to operate efficiently under loose coupling conditions. Coupling between souce or load coils to their corresponding resonant coil (k_{12}, k_{34}, and k_{56}) is mostly form factor dependant. The coupling coefficient is typically high (> 0.1) because of the physical nature of having both coils placed in close proximity within the device.

The concept behind time division multiplexing is to transfer power to a single receiver exclusively. Each receiver's resonant coil is detuned selectively when tightly
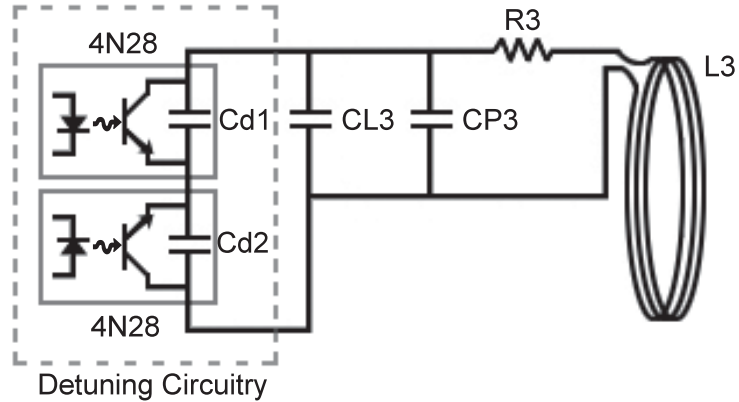
Fig. 3.9. Receiver resonant coil detuning circuitry.

coupled eliminating the effect of frequency splitting. Two important aspects of TDM are the detuning method and how RX coils are synchronized.

3.4.1 Detuning Circuitry

For a two receiver scenario, one of the receivers is detuned by shorting the coil which removes its resonant capabilities. It is essentially a shorted inductor coil with parasitic resonance.

Fig. 3.9 describes the detuning circuitry implemented with two back-to-back 4N28 opto-isolators which are enabled simultaneously with a shared detuning signal. The opto-isolator is used as a switch with large ground isolation between the resonant coil and the control logic circuitry. The reason behind doing this is to reduce the amount of resonant perturbation due to increased parasitic capacitance. The phototransistor switch is enabled through a gallium arsenide infrared LED. In [32], a detuning circuit is used only when the receiver is fully charged to increase power tranference for receivers still in need of power. The detuning technique used in our work requires fewer components and is easier to implement. If power MOSFETs are used [32] for detuning, an external diode pointing at the opposite direction of the body diode is needed due to the body diode of the FET and the AC nature of the received signal.
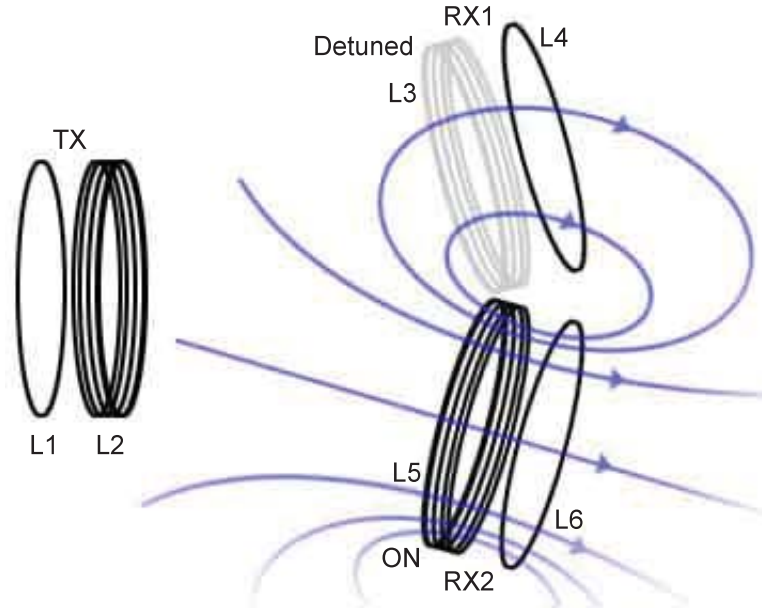
Fig. 3.10. Illustration on how synchronization is kept in detuned mode. Detuned receiver RX_1 is receiving the synchronization signal from resonant coil, L_5 of RX2.

This method is more complex as the diode has non-linear junction capacitance which varies with voltage. It only conducts in a single direction and would require a set of identical components in the opposite direction.

The 4N28 component was chosen for theoretical purposes and has inherit limitations due to low V_{CE} and V_{EC} max limits of 30V and 7V. The reason behind having back-to-back optoisolators is to increase the 'off' state max limit voltage to V_{CE} instead of V_{EC} in the reverse direction.

It is important to include the parasitic capacitance of the entire detuning circuitry. The addition of the series 4N28 output capacitance, C_{d1} and C_{d2}, will add to the overall capacitance of the resonant coil. C_L is the added lumped capacitor value with C_P the parasitic capacitance of the resonant coil. The total or effective capacitance, C_{eff}, of the resonant coil is given by

$$C_{eff} = \frac{C_{d1}C_{d2}}{C_{d1} + C_{d2}} + C_{L3} + C_{P3}. \tag{3.10}$$

The effective capacitance values of C_2, C_3 and C_5 are stated in Table 3.3. During detuning, in an ideal case, one can consider the transistor switch as a short and will detune the resonant coil to the coil's self resonance. Since the resonant coil has a high Q-factor, slight changes in the capacitance alone will be sufficient to detune the coil. Detuning is only implemented at each receiver's corresponding resonant coil and not at the load coil.

3.4.2 Synchronization Technique

The TDM technique relies on proper synchronization of the detuning signal for each receiver. Each resonant coil needs to be detuned and powered at its specific time slot. During detuning, the power received at the receiver is extremely low such that no power is transferred from its corresponding detuned resonant coil. However, due to the close proximity of the two receivers, the nearby non-detuned resonant coil can be utilized for a continued synchronization signal. The received sync voltage will typically be low and will depend on how tight cross coupling coefficients k_{36} and k_{45} are between receivers. Fig. 3.10 provides a visual explanation on how a detuned receiver obtains the synchronized signal. The TDM method only detunes the resonant coil of the receiver at L_3 or L_5 while leaving its corresponding load coil of L_4 or L_6 unchanged.

At tight coupling, both RXs will be in close proximity to each other and this provides a reasonable assumption of both RXs being equidistance to the TX resulting in a locked received signal in terms of frequency and phase. The detuned receiver would be able to use coupling between the adjacent non-detuned resonant coil with its load coil. The physical configuration of the RX coil either in planar or solenoidal form dictates how tight this coupling is. Resonant and load coils are separated at a distance d_{34} or d_{56} with similar radii solenoidal coils. If the resonant pairs are placed on a planar plane for reduced z-height, the TDM method will show substantial improvements due to tighter coupling between RX coils.
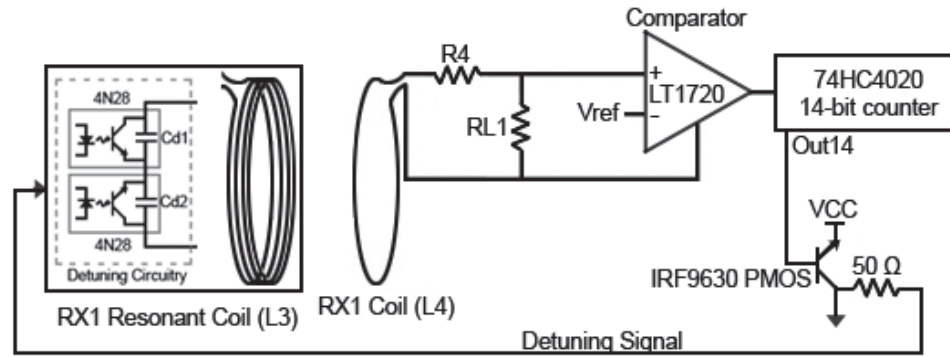
Fig. 3.11. Receiver synchronization circuitry for each receiver coil pair

Fig. 3.11 describes how synchronization is implemented with the detuning circuitry in both receive pairs. The output of the receiver is fed into a comparator (LT1720) with a reference voltage (V_{ref}) of 33mV. Having the voltage threshold at this level has advantages in terms of mitigating noise when no TX is present and also for automatic adjustment of the synhronization circuitry. The threshold value is physically dependant on the receiver coil's coupling and should be tuned such that an adjacent coil can be detected without having false triggers. The output of the comparator is fed into a 14-bit counter which outputs a divided frequency. This is to acquire a slower switching logic signal to turn on and off the detuning circuitry. The most significant output, Out_{14} is chosen such that the receive frequency of 8.4MHz is divided by 2^{14}. A detuning frequency (f_{det}) of approximately 512 Hz is used as an enable signal for the detuning circuit's optocouplers. Since the output of the counter has a max current limit of 20mA, a PMOS switch is used to power the infrared LED of both optocouplers. Providing enough power for the LED is important to ensure maximum current transfer ratio for efficient detuning.

The comparator, counter and detuning circuitry is powered from each receiver's battery for simplicity. For a two receiver TDM solution, one of the receivers uses an inverted reference to receive a 180° out-of-phase signal for detuning. This ensures a 50% duty cycle on and off time for both receivers. This technique of achieving the inverted signal is done for experimental purposes. Additional hardware can be

Table 3.3
Parameter Values

Par.	Value	Par.	Value	Par.	Value	Par.	Value
R_S	50 Ω	L_1	.30 μH	k_{12}	.175	k_{34}	.175
R_1	.053 Ω	L_2	6.10 μH	k_{13}	.0035	k_{35}	.06
R_2	.265 Ω	L_3	6.11 μH	k_{14}	.0025	k_{36}	.02
R_3	.265 Ω	L_4	0.3 μH	k_{15}	.0035	k_{45}	.02
R_4	.053 Ω	L_5	6.12 μH	k_{16}	.0025	k_{46}	.01
R_5	.265 Ω	L_6	.3 μH	k_{23}	.00425	k_{56}	.175
R_6	.053 Ω	C_2	58.9 pF	k_{24}	.0035		
R_{L1}	100 Ω	C_3	58.8 pF	k_{25}	.00425		
R_{L2}	100 Ω	C_5	58.7 pF	k_{26}	0.0035		

added to achieve different duty cycles if more receivers are present. It is important to note that the received signal at similar distances amount to a locked signal in terms of frequency and phase using the same reference point. The only caveat is that the counter for each receiver pair is not synchronized in terms of their initial counting stages. However, using an appropriate reference signal at the comparator helps synchronize this initial counting stage offset. Basically, both receivers will be counting at a slightly different frequency where it will start drifting due to missed transitional signals below the reference signal of the comparator until an equilibrium point is reached corresponding to its received original frequency of 8.4MHz.

3.5   Simulation and Experimental Results and Analysis

The experimental setup for tightly coupled receivers is shown in Fig. 3.12. Parameters for the entire setup used for simulation are shown in Table 3.3. Methods of determining the parameters are described in [1]. The distances d_{12}, d_{34} and d_{56} between the driver/load coil to their respective resonator coil were set at 4.2 cm with the distance between TX and RX resonant coil, d_{23} and d_{25} placed at 28cm apart. The transmitter source, V_S has a frequency of 8.4 MHz coinciding with the coil's
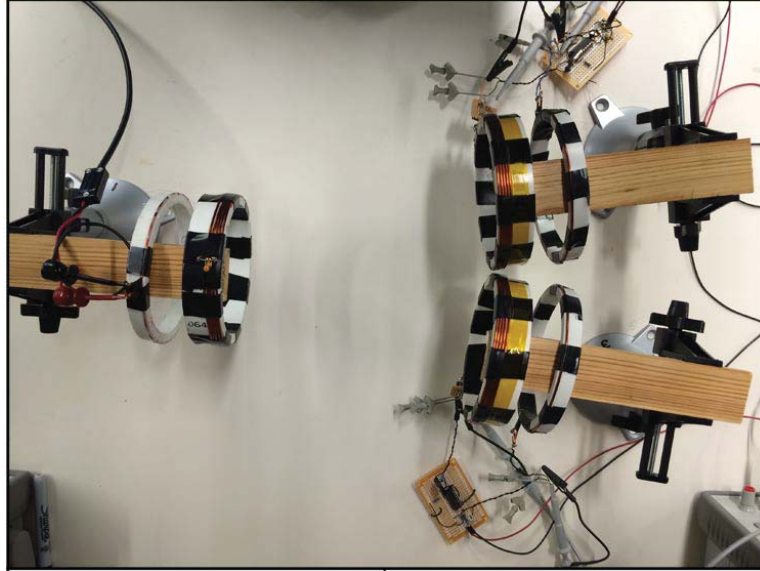
Fig. 3.12. Experimental setup for receiver tight coupling

resonance. After measuring the inductance of the resonator coil, C_{eff} is derived from the known RLC resonant frequency equation as such

$$C_{eff} = \frac{1}{4\pi^2 f_0^2 L}. \tag{3.11}$$

f_0 is the resonant source frequency and L is the inductance value of the coil. The theoretical value of the capacitance calculated is used as reference for determing the lumped capacitance value since the coil itself introduces parasitic capacitance. Careful adjustments of the capacitor are needed due to the resonator's high Q-factor. The Q-factor is dependent on the resistance of the coil as well as the corresponding inductance and capacitance as shown by

$$Q = \frac{\omega L}{R} = \frac{1}{R}\sqrt{\frac{L}{C}}. \tag{3.12}$$

k_{35} is the coupling coefficient between RX resonant coils and is the key factor in determining how far the frequency splits away from the source frequency. The higher the coupling, the further away the second peak is from resonance. Even though a peak is present at resonance, the overall transfer function is reduced significantly.
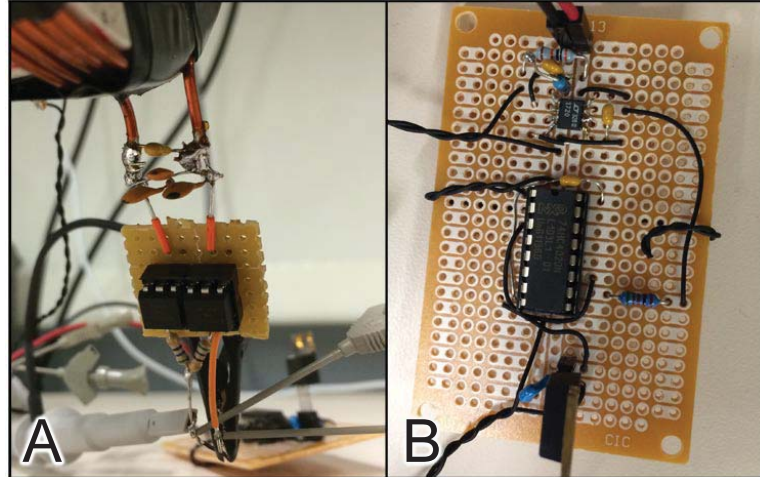
Fig. 3.13. Picture of (A) Detuning circuitry and (B) Synchronization circuitry

If planar coils are used, coupling between receivers is of concern since devices can easily be stacked on each other. Our work focuses on a solution to ensure that wireless power transfer still functions due to a minimum voltage requirement for proper rectification. However, there is a 50% reduction of total power transferred as the receiver is switching at 50% duty cycle.

TDM can be understood as if the detuned resonant coil is non-existent within the system. For simulations, there are two ways of obtaining the equivalent SISO ($N = 1$) transfer function assuming negligible cross coupling by either assigning zero coupling to any interactions with the designated detuned resonant coil or use a drastically different lumped capacitor value. Both methods will result in the same transfer function as

$$I_{N,RX} = \frac{jw^3 M_{12}^2 M_{23} \, V_S}{w^4 M_{12}^4 + Z_{11} Z_{22}^2 Z_{66} + w^2 Z_{11} Z_{22} M_{12}^2 + w^2 Z_{22} Z_{66} M_{12}^2 + (N) w^2 Z_{11} Z_{66} M_{23}^2}. \tag{3.13}$$

(3.13) is an ideal simplified general transfer function equation for N receivers with vanishing interaction between them. It is important to understand that in an ideal condition, charging two receivers will always have lower simultaneous received power
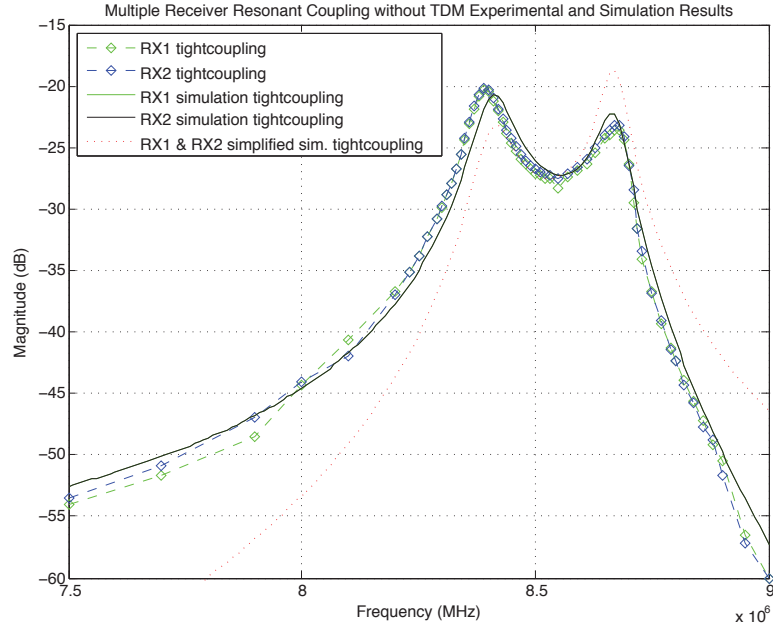
Fig. 3.14. RX-RX resonant coil tightly coupled transfer function $|V_{L1}|$ without TDM implementation

for two receivers when compared to the single receiver case. Hence, at a tightly coupled condition, detuning will tremendously increase the amount of power received when switched to SISO. The received current is ultimately increased as the variable N reduces to 1 while also eliminating the added denominator **x** term (3.14) in (3.4) explained in the Section 3.5.2.

Due to the fixed physical setup between resonant and source/load coil, the tightest coupling between receiver resonant coupling can be seen in Fig. 3.12.

3.5.1   Tight RX-RX coupling without TDM implementation

Fig. 3.14 shows simulation and experimental transfer function results for a tightly coupled RX system without TDM implementation. Frequency splitting is the effect of tight RX-RX coupling at a k_{35} value of 0.06. Peaks are seen at the source frequency of 8.4MHz and 8.67 MHz, respectively. Even though resonance is seen at the driving frequency, the overall transfer function is lowered considerably by more than 9dB
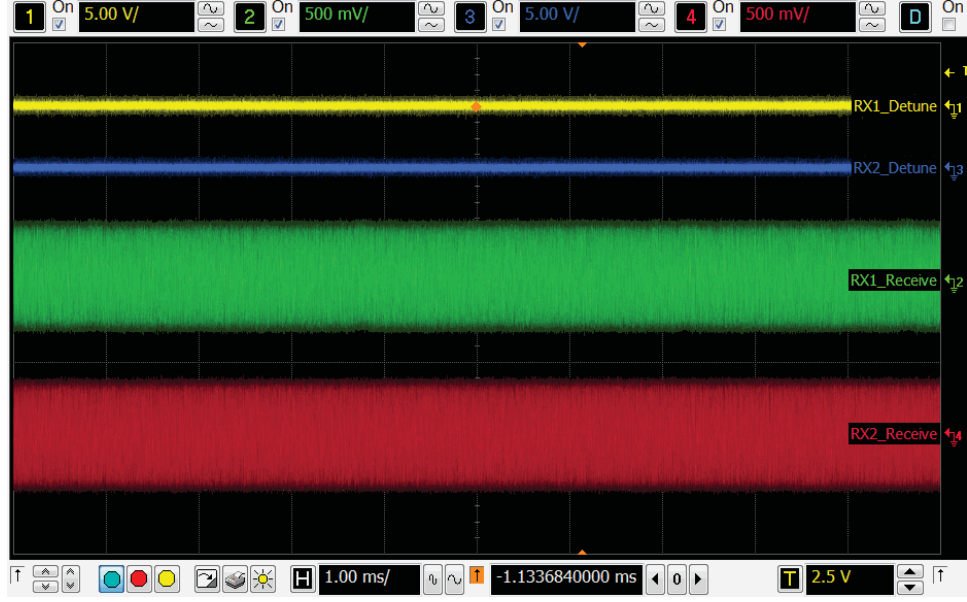
Fig. 3.15. RX load output in tight RX-RX coupling without TDM

when compared to the SISO case seen in Fig. 3.17. This results in rectification issues when the voltage received is much lower than the intended input voltage. If a low drop out (LDO) regulator is used at the back end, this could result in a non-workable solution where the received DC voltage after rectification is lower than its minimum input voltage.

A general 1TX - NRX case (3.13) assumes negligible coupling between N receivers. As the number N of receivers increase, the assumption of having negligible RX-RX coupling becomes less achievable. The simplified Equation (3.4) represents the 1TX-2RX case of $N = 2$ receivers with significant coupling ($k_{35} > 0.01$). This tight RX-RX coupling results in an additional $\mathbf{x}$ term, given by

$$\mathbf{x} = jM_{35}(-M_{12}^2 Z_{66} w^3 - Z_{11} Z_{22} Z_{66} w) \tag{3.14}$$

in the denominator of (3.4).

RX-RX coupling coefficient of k_{35} increases as receivers are brought closer to each other. Hence the value of $\mathbf{x}$ increases due to a higher M_{35} value which in turn reduces
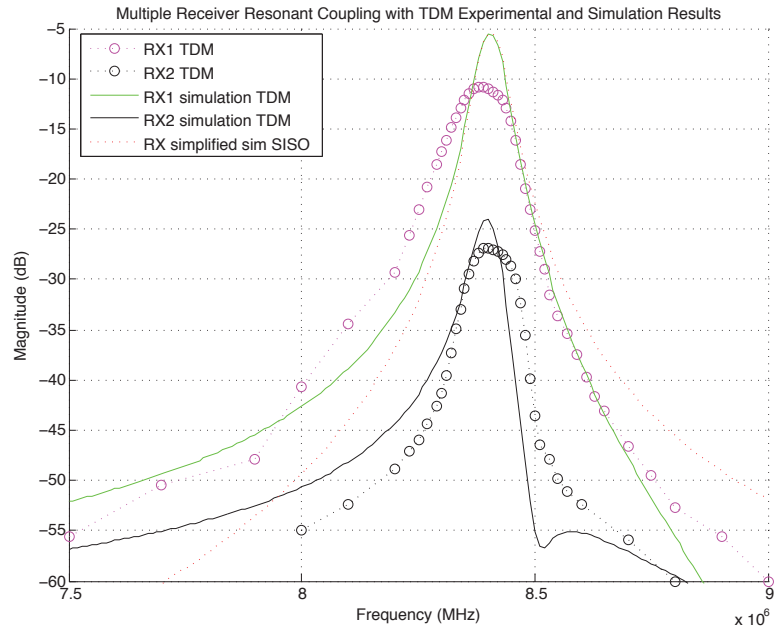
Fig. 3.16. Experimental and simulation transfer function $|V_{L1}|$ results for an RX-RX tightly coupled case with TDM implementation

the overall induced current at the receiver. The idea of TDM, is to eliminate this added **x** factor. Another important benefit of TDM is the fact that (3.13) improves by having $N = 1$ during detuning which mimics a SISO case. During detuning, the resonance coil can be disregarded as if it is invisible to the overall system.

Fig. 3.15 shows experimental received voltages at both loads RX_1 and RX_2 without any detuning method. The source frequency is operating at the system's resonant frequency of 8.4MHz. The peak to peak voltage (V_{pp}) seen at both RX_1 and RX_2 is measured to be 760mV with an equivalent V_{RMS} value of 268.7mV. Power transferred to each receiver with a fixed 100Ω load is calculated to be 0.72mW. It will be shown in the next subsection that received power can be increased despite operating only half the time.

Fig. 3.17. RX load output in tight RX-RX coupling with TDM method

3.5.2   Tight RX-RX coupling with TDM implementation

Fig. 3.16 shows simulation and experimental transfer function results for a tightly coupled RX system with TDM implementation. The magnitude of RX_1 with RX_2 detuned shows an increase of approximately 9dB. Fig. 3.17 shows the experimental measurement at both loads in TDM mode. The time division or allocated time for each coil is set at a 50% duty cycle with a synchronization frequency of 512Hz. The received 'ON' voltage is measured to be 2239.2mV$_{pp}$ with an 'OFF' voltage or detuned voltage of 364.8mV$_{pp}$. The power transferred to a tuned load has a V_{RMS} of 791.7mV with 6.26mW power transferred to the load. Since the load is switching on at half the frequency, the average power received is halved at 3.13mW. A simple division by two works for a 50% duty cycle detuning signal. The average power dissipated at the load can be calculated by

$$P_{RX} = \frac{V_{RMS}^2}{R_L} = \frac{1}{R_L} \left[\frac{1}{T} \int_0^x V_p^2 \ \sin(2\pi f_0 t)^2 dt \right] \tag{3.15}$$

where a 50% duty cycle detuning signal with period T will have an x value of $T/2$.

Table 3.4

TDM Received Power Improvement

TDM	RX V_{rms}	Trans.Func.	RX Avg. Pow.	% Power Inc.
No	268.70 mV	-20dB	0.72mW	-
Yes	791.68 mV	-11dB	3.13mW	335%

In (3.15), T has a value of $1/f_{det}$ $(1/512 = 2ms)$ where power is transferred during the first $T/2$ seconds. Despite operating at half the amount of time, there is a 4.3 times increase of received average power in T seconds when compared to the always detuned case shown in the previous subsection. Theoretically, having power equally distributed between eight receivers $(T/8)$ will still have more average power transferred at 0.78mW each. This is with the assumption that all eight receivers are equidistance between TX and RX and have negligible coupling between each other.

Fig. 3.17 shows RX_1 and RX_2 measurements with TDM implemented. It is perfectly synchronized with the detuning signal of each receiver differing by 180°. 'RX1_Receiver' (green) and 'RX2_Receiver' (red) is the voltage drop at their corresponding load. The transfer function plotted in dB is used to show that regardless of the actual source voltage value, it will scale accordingly. Ideally, if there were no component limitations, one could insert a relatively high valued voltage source with the output scaling according to the corresponding transfer function plot. In this case, at resonance, the received magnitude is approximately -11dB compared to -20dB for the tightly coupled case without TDM.

Table 3.4 gives a summary of the improvements seen using TDM. Columns 'RX V_{rms}' and 'Trans. Func.' in the table are instantaneous values while 'RX. Avg. Pow.' is the average power received. There is a 335% increase in received average power when TDM is implemented. The improvement is highly dependant on how tight the coupling is between receivers. Tight coupling of the receivers is needed for proper TDM synchronization as the detuned receiver depends on cross coupling between resonant and load coils.
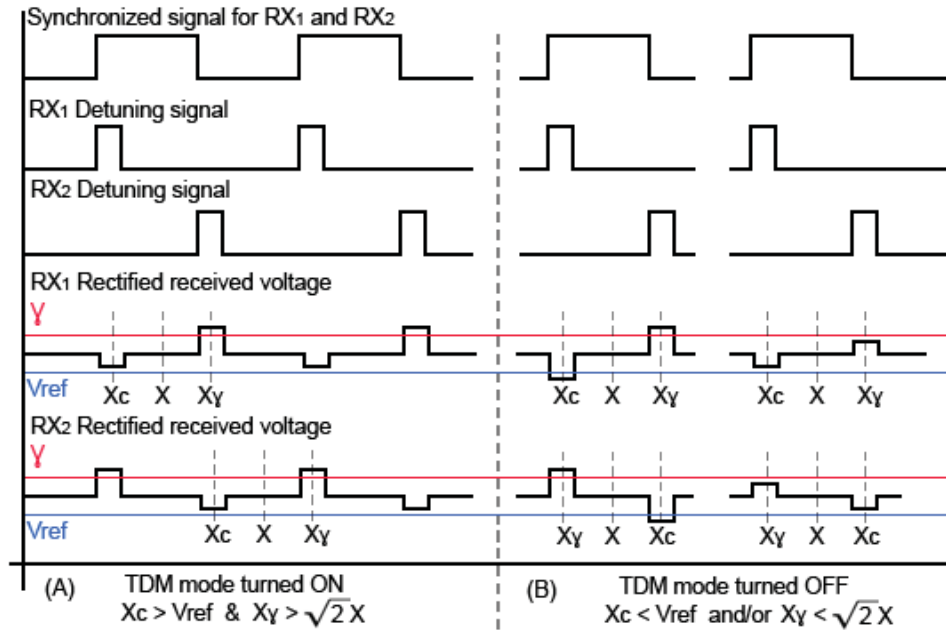
Fig. 3.18. Timing visualization on how thresholds γ and V_{ref} are compared for both receivers during TDM monitoring.

3.5.3 TDM Scheduling Implementation Strategy

The dissipated power at the load without TDM, P, and with 50% TDM, P_{TDM}, can be shown as:

$$P = \frac{X^2}{R_L}, \ P_{TDM} = \frac{(Xa)^2}{2R_L} \tag{3.16}$$

where X is the received RMS voltage at a tightly coupled receiver without TDM and a the multiplication factor introduced to indicate the increase in voltage with TDM. The TDM average power equation P_{TDM} in (3.16) is divided by two due to detuning. If a has a value of $\sqrt{2}$ after detuning, the resultant power transferred is the same with and without TDM. As receivers are brought closer together, TDM should be implemented only when $a > \sqrt{2}$. Using experimental results from Section 3.5.2 as an example, the multiplication factor a has a value of 2.95 which is higher than $\sqrt{2}$. This is obtained by dividing the TDM received RMS voltage of 791.68mV with the non-detuned voltage of 268.7mV.

The next practical step is to determine when to start TDM. The experimental data shown in Section 3.5.2 had an always on TDM mode. WPT standards such as A4WP [34] and Qi [35] have a communication method using load modulation to handshake between TX and RX. Assuming two receivers are powered simultaneously, the TX will let both receivers know there are a total of two systems being powered. Once this is known, each receiver will start to monitor received voltage levels and start detuning at different time slots. Since they share the same synchronized frequency, simultaneous detuning can be avoided. An indicator signal from the detuning circuit's comparator threshold (V_{ref}) is also needed to check if the receivers are close to each other. A threshold voltage value, γ is used to determine if detuning is suitable given the amount of coupling between the receivers:

$$\gamma_i = aX_i, \ a = \sqrt{2} \tag{3.17}$$

The subscript i indicates different values received in time when the threshold is checked during non-detuning and detuning.

As long as two receivers are tightly coupled and are in communication with the transmitter, each receiver will monitor its voltage received in detuning and non-detuning mode to compare with the comparator, V_{ref} threshold and updated γ threshold. If the receivers are moved away from each other, the initial indicator from the comparator will disable TDM. At a tightly coupled scenario, if the received voltage is below γ during checks, the receiver should halt TDM as it will have a lower received average power. Monitoring initiates only when the transmitter indicates another receiver is present. Fig. 3.18 provides a visual explanation on when each receiver should sample the received voltage X, X_c and X_γ before and during detuning of each receiver. TDM is turned on if $X_c > V_{ref}$ and $X_\gamma > \sqrt{2}X$ and is turned off if $X_c < V_{ref}$ and/or $X_\gamma < \sqrt{2}X$ occurs. If a has a value between 1 and $\sqrt{2}$, TDM should not be initiated. The 2.95 value of a showed in Section 3.5.2 shows a received voltage higher than the γ threshold of 380 mV which is the multiplication of $\sqrt{2}$ with an X value of 268.7mV. Hence, TDM implementation increases the average received power.

(A) RX2 is on with RX1 and RX3 detuned | (B) RX1 and RX3 are on with RX2 detuned
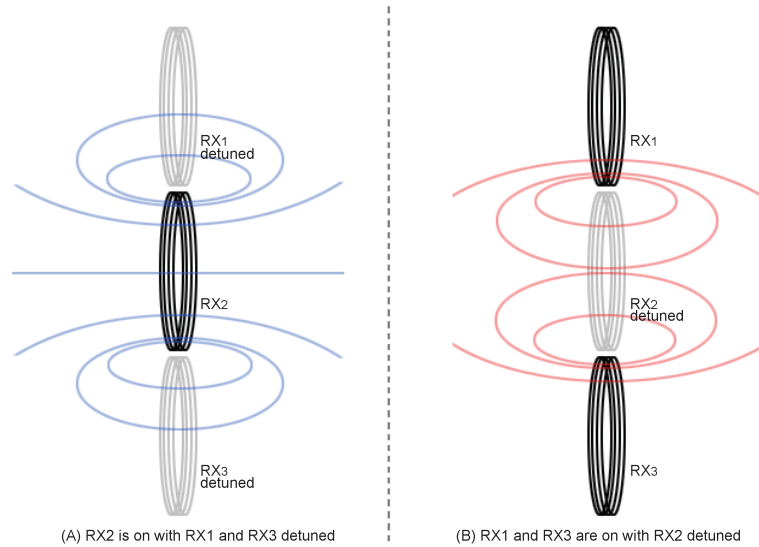
Fig. 3.19. Dynamic TDM enhancement for three receivers.

Optimizing the detuning time for monitoring and how frequently it is done is left for future work.

3.6 TDM enhancements and Future Work

3.6.1 Dynamic TDM mode for N receivers

Most of the TDM work was shown in the simplest receiver coupling case which has only one transmitter and two receivers. If three receivers are present, time sharing between three devices further divides the allocated power. Hence, as the number of receivers, denoted by N, increases, the receive power is reduced by a factor of N.

However, tight receiver coupling often involves close distances and not all receivers share the same distance to each other. If three receivers, RX_1, RX_2 and RX_3 are closely aligned in a line with RX_2 positioned in the middle, RX_1 and RX_3 can be turned on simultaneously as they are not tightly coupled. For RX_2, it will be tightly coupled to both RX_1 and RX_3. Fig. 3.19 helps explain the intended three receiver TDM dynamic mode enhancement. The ability to determine the coupling between
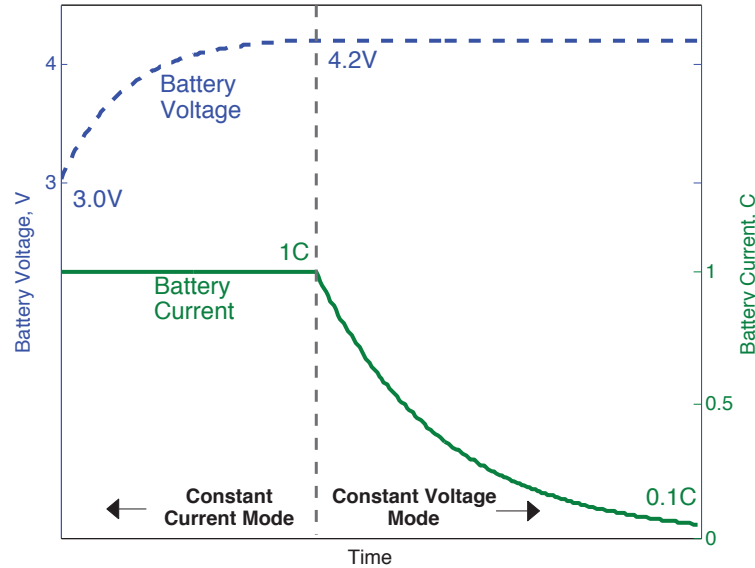
Fig. 3.20. A typical lithium-ion battery charging profile. Two common modes of constant current and constant voltage is shown versus time.

receivers would dramatically enhance this proposed TDM scheme. Simultaneous powering of receivers which are not tightly coupled have improved overall efficiencies.

The dynamic TDM mode would require nearby coil information to determine which coil is tightly coupled. If a communication link between receivers can be established, then knowing each receiver's distance between each other and synchronously sharing time bandwidth could lead to increased efficiencies when tightly coupled.

3.6.2   Tunable TDM detuning based on receiver battery capacity state

Sections 3.4 and 3.5 showed improved power transfer perfomance using a 50% duty cycle between two tightly coupled receivers. The method of detuning was fixed at equal charging times and was used as a proof-of-concept on how TDM in general could be used in a tightly coupled receiver scenario. Further enhancements by using an adjustable detuning signal which takes into account the charge state of the receiver's battery could boost charging times by intelligently partitioning the amount of power

needed. For example, if a receiver is fully charged in a two receiver case, the unit should be detuned completely and allow a 100% duty cycle charge time for increased power transfer to the other receiver.

Fig. 3.20 shows a typical lithium-ion battery charging profile. Two typical modes of charging consist of the constant current and constant voltage mode. The battery current is constant at the latter stage and tapers off exponentially in the constant voltage mode. It is assumed that the transmitter knows the battery state of the receivers. If the voltage reading at the receiver's battery is lower than the constant voltage threshold (4.2V for the example in Fig. 3.20), a max 1C charge is typically sourced into the battery. A 1C charge is equivalent to a charge current of one times the rated battery capacity. For example, a 2200mAh battery pack would have a 1C charge equivalent of 2.2A. Constant current mode is also commonly referred to as fast charging and typically ends at a 70% charge state for the battery. For simplicity, for N receivers in constant current mode, dividing the duty cyle by N would allow equal charging times assuming equivalent battery capacity. This is easily implementable as the charge current is constant and does not require monitoring until the threshold voltage is reached.

The tunable TDM enhancement would prove beneficial if one or more of the receivers are operating in the constant voltage mode where the power needed is lower. In practice, there are limitations to the total output power a charging station can provide. For the Qi standard, the receiver sends control packets to adjust the received power level. Based on this information, a simple detuning algorithm can be used as shown by

$$D_i = \frac{W_i}{\sum_{i=1}^{N} W_i} (100\%) \tag{3.18}$$

where D_i is the non-detuning time allocation of the i-th receiver. W_i represents the requested power information sent by receiver i to the transmitter. N represents the total number of receivers seen by the TX. The detuning signal is an active high signal where the coil is charged at the low input and detuned at the high input of the signal.
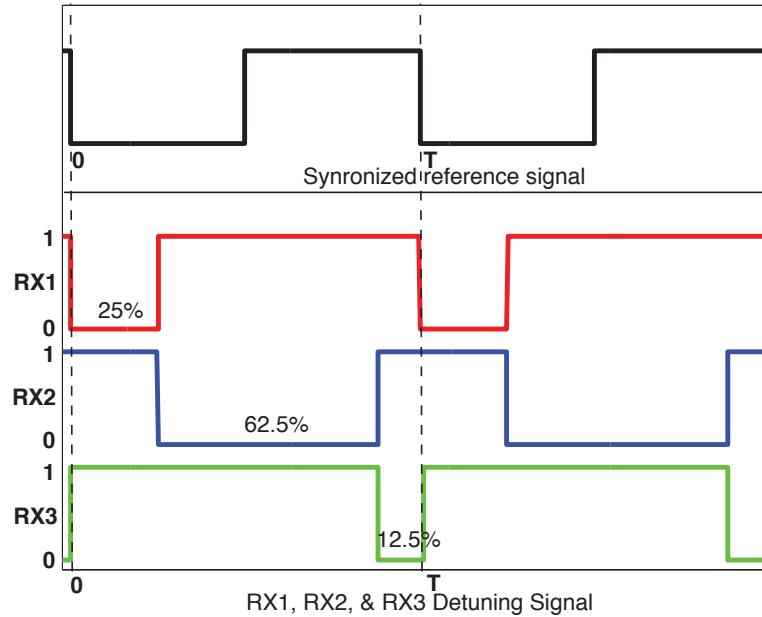
Fig. 3.21. A tunable TDM example for three receivers RX_1, RX_2 and RX_3 with a two, five, and one watt power requests. A low signal indicates charging or powering in which the resonant coil is not detuned.

Fig. 3.21 shows an example for $N = 3$ receivers with W_1, W_2 and W_3 requested power values of 2W, 5W and 1W respectively. Plugging the requested power numbers in (3.18) gives the corresponding charging times of $[0,0.25T]$, $[0.25T,0.875T]$ and $[0.875T,T]$ respectively. T is defined as the TDM periodic cycle time. If the power source is constrained to a total available power of 5W, using (3.7), the received power will be divided to 1.25W, 3.125W and 0.625W, respectively. The TX charging station will provide the necessary time slots based on this information. Once D_i is known, the TX needs to let each receiver know their designated detuning times. Proper synchronization between receivers is needed to ensure unique turn on times for each receiver.

3.7   Conclusion

The coupled magnetic resonance (CMR) technique increases operating spatial freedom with enhanced efficiencies at lower coupling coefficients. However, coupling between receivers gives rise to new challenges as resonator coils are more susceptible in tight coupling conditions. Degradation of received power levels is seen in a tightly coupled multiple receiver case as interfering magnetic fields reduce overall induced current at the receivers. A time division multiplexing scheme is developed to mitigate this effect and has been proven theoretically and experimentally. As support for multiple receivers gains traction, the TDM method provides a compelling solution for tightly coupled receivers.

4. FUTURE WORK: TRADEOFF ANALYSIS OF SIMULTANEOUS POWER AND INFORMATION TRANSFER

4.1 System Model overview

Fig. 4.1 shows the basic circuit model of a coupled magnetic resonance coupling system. It is a representation of a SISO system with a source coil L_1 and a load coil of L_4. Both transmitter and receiver consist of their corresponding resonant coil of L_2 and L_3. The simulation parameters are based on the actual experimental coils used in Chapters 2 and 3. Table 2.2 and Table 3.3 are used for all resistance, capacitance and inductance values.

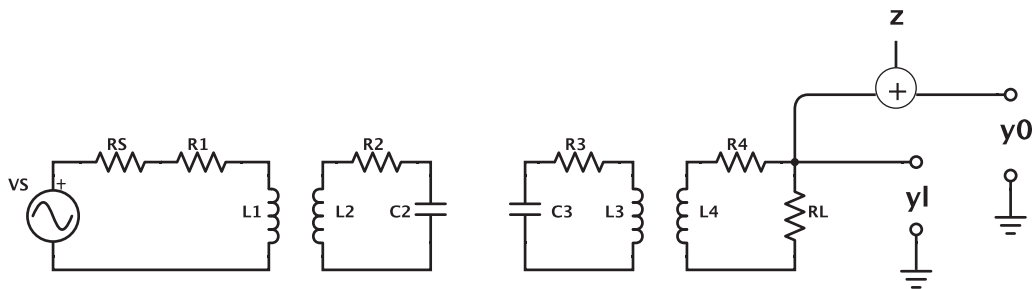Fig. 4.1. A coupled magnetic resonance inductive circuit model.

The model is viewed as a frequency selective channel with AWGN noise added at the load [36] . The system equation is described as

$$y_0(t) = y_l(t) + z(t) \tag{4.1}$$

where y_0 represents the output seen after adding AWGN noise, z of N_0 variance, to the output seen directly at the load. The main difference between the CMR setup and

the inital investigation by Pulkit et al. [36] is primarily the total system efficiency. The efficiency of the system termed $\eta(f)$ is directly related to the fading parameter, $h(f)$ as is commonly used in wireless communication theory. It is the total power delivered, P_{del} divided by the total available power, P_{avl} as given by

$$\eta(f) = |h(f)|^2 = \frac{P_{del}(f)}{P_{avl}(f)}. \tag{4.2}$$

The power consumed at the receiver or delivered power, P_{del} is the product of the load resistance, R_L with the squared value of the received RMS current, I_4:

$$P_{del} = |I_4|^2 R_L. \tag{4.3}$$

The total available power, P_{avl} can be calculated by

$$P_{avl} = |I_1|^2(R_S + R_1) + |I_2|^2 R2 + |I_3|^2 R3 + |I_4|^2(R4 + RL) \tag{4.4}$$

which is equivalent to the total power dissipated across all resistances. The output of the power source will depend on the coupling or load seen from the source side. The RMS current $I_1 \ldots I_4$ for each loop is given by

$$\begin{bmatrix} I_1 \\ I_2 \\ I_3 \\ I_4 \end{bmatrix} = \begin{bmatrix} Z_S & jwM_{12} & jwM_{13} & jwM_{14} \\ jwM_{12} & Z_R & jwM_{23} & jwM_{24} \\ jwM_{13} & jwM_{23} & Z_R & jwM_{34} \\ jwM_{14} & jwM_{24} & jwM_{34} & Z_L \end{bmatrix}^{-1} \begin{bmatrix} V_S \\ 0 \\ 0 \\ 0 \end{bmatrix} \tag{4.5}$$

where the individual impedances in the Z-matrix in (4.5) are given by

$$Z_S = j\omega L_1 + R_S + R_1$$
$$Z_R = j\omega L_2 + R_2 + \frac{1}{j\omega C_2}$$
$$Z_L = j\omega L_4 + R_L + R_4$$

with the mutual inductance, M_{kl} given by (2.3). Solving for each individual RMS current in (4.5), it can be plugged into the efficiency equation given known coupling coefficients as shown by

$$\eta = \frac{|I_4|^2 R_L}{|I_1|^2 (R_S + R_1) + |I_2|^2 R2 + |I_3|^2 R3 + |I_4|^2 (R4 + RL)}. \tag{4.6}$$

4.2   Capacity formulation

The capacity equation for the inductively coupled scheme uses Shannon's AWGN channel capacity based on the receiver's signal to noise ratio. Work by [36] was the first to consider the problem of simultaneous information and power transfer for a WPT system. The following equation was derived on the assumption that the signal received at the load is corrupted with thermal noise which is Gaussian in nature. However, unlike in communications, the power being sent is much higher than the thermal noise seen resulting in very high SNRs. The main problem is the fact that the system source frequency in a CMR-type WPT system typically uses zero bandwidth which pumps maximum power at a fixed frequency. The bandwidth of the system is zero if a single sinusoid is used mainly for power transfer.

The capacity equation can be written as:

$$C = \Delta_f \sum \log_2(1 + SNR) = \Delta_f \sum_{i=1}^{n} \log_2(1 + \frac{\eta_i P_i}{N_0}) \tag{4.7}$$

with η_i and P_i corresponding to the system's effeciency and allocated power for each channel. Δ_f is the fixed bandwidth value used for each i-th slot. Since the analysis is done in the discrete case, the smaller Δ_f value will provide better correlation with the continous case.

The capacity shown in (4.7) is to be optimized with the following constraint of having the total sum for each i-th transmit slots, P_i bounded by the total available power, P_{avl} given by

$$\sum_{i=1}^{n} P_i \le P_{avl}. \tag{4.8}$$

The optimization result of using only an available power constraint is the waterfilling solution at a given delivered power value. Having an increased delivered power above

this value will result in less information being sent. Hence, there is a tradeoff between having maximum information rate or maximum power delivered.

The delivered power constraint is of the following

$$\sum_{i=1}^{n} \eta_i P_i \geq P_{del} \tag{4.9}$$

with η_i the system efficiency at the i-th channel. Using the following two chosen constraints of bounding the total power, P_{avl} and a minimum bound for the delivered power, P_{del} the capacity is

$$C(P_{del}, P_{avl}) = \max_{\sum_{i=1}^{n} \leq P_{avl}, \ \sum_{i=1}^{n} \eta_i P_i \geq P_{del}} \sum_{i=1}^{n} \log_2(1 + \frac{\eta_i P_i}{N_0}). \tag{4.10}$$

The optimized input power for each i-th channel P_i^* can be found using the Langrangian method by introducing non-negative multipliers λ and μ as such

$$\Lambda = \sum_{i=1}^{n} \log_2 \left(1 + \frac{\eta_i P_i}{N}\right) - \lambda \left(\sum_{i=1}^{n} P_i - P_{avl}\right) + \mu \left(\sum_{i=1}^{n} \eta_i P_i - P_{del}\right) = 0. \tag{4.11}$$

To obtain the waterfilling solution, (4.11) is differentiated with respect to P_i and is set to zero as given by

$$\frac{d\Lambda}{dP_i} = \frac{\eta_i}{N \ \log(2) \left(1 + \frac{\eta_i P_i}{N}\right)} - \lambda + \mu\eta_i = 0 \tag{4.12}$$

resulting in the optimum power allocation P_i^* for each i-th channel as such

$$P_i^* = \left(\frac{\log_2(e)}{\lambda - \eta_i \mu} - \frac{N}{\eta_i}\right)^{+}. \tag{4.13}$$

The superscript '+' in (4.13) indicates a minimum value of zero or a positive number

as the transmit power cannot have negative values in practice. If there is no P_{del} constraint, the resulting transmit power, P_i^* will result in the maximum information rate at the current system setting. If the maximum value of information is wanted, the μ value is set to zero indicating only the power source constraint which reduces (4.13) to

$$P_i = \left(\frac{\log_2(e)}{\lambda} - \frac{N}{\eta_i} \right)^+ . \tag{4.14}$$

4.3   Simulation Results and Analysis
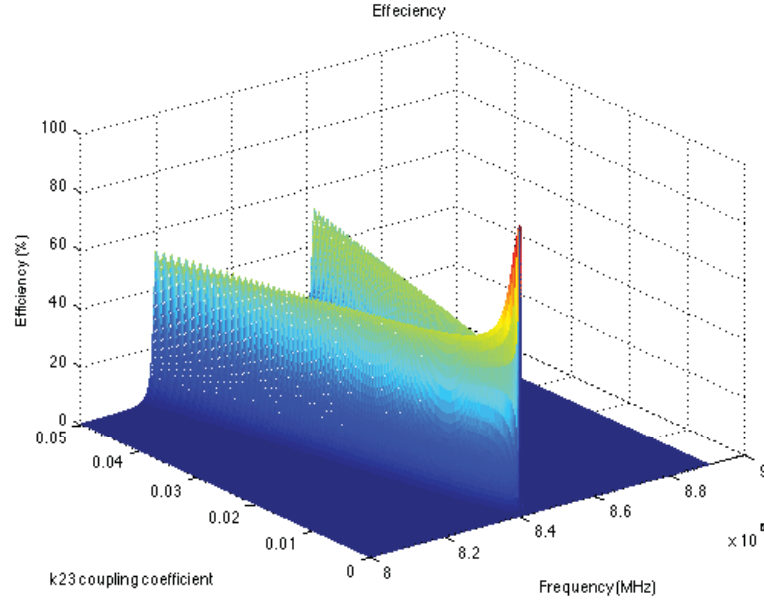
Fig. 4.2. Efficiency plot vs. frequency and k23 coupling coefficient (distance)

The setup used for simulation is a coupled magnetic resonance system in a single-input single-output case. Before looking into the tradeoffs between information and power transfer rates, an explanation of the system in terms of its efficiency and transfer function is needed. There are three different regions in which the TX and RX can operate, they are the critically coupled, overcoupled and undercoupled region. The overcoupled region is where frequency splitting occurs. The transfer function will

result in two resonant peaks that deviate from the original resonant frequency of both the resonant coils and power source.

Fig. 4.2 shows a 3D plot of the efficiency vs. frequency and the k_{23} coupling coefficient. This coupling coefficient represents the distance between TX and RX. The efficiency plot starts to exhibit frequency splitting at a k_{23} coupling coefficient value of 0.0029. Hence, with this system, critical coupling occurs at coefficient value of 0.0029 with undercoupling occuring at k_{23} values less than 0.0029 and overcoupling happening at values above 0.0029. If looked closely at Fig.4.2, the efficiency at the two resonant peaks is 55% and 50% respectively. It starts to plateau at a value above a k_{23} coupling coefficient of 0.007. This is important as the capacity is calculated based on the efficiency of the system as the power needs to be constrained. If observed closely again, the efficiency value peaks at extremely low coupling coefficients as if operating at a far distance will provide even higher transfer rates. This of course is false as the power transferred is extremely low even though the efficiency is high.
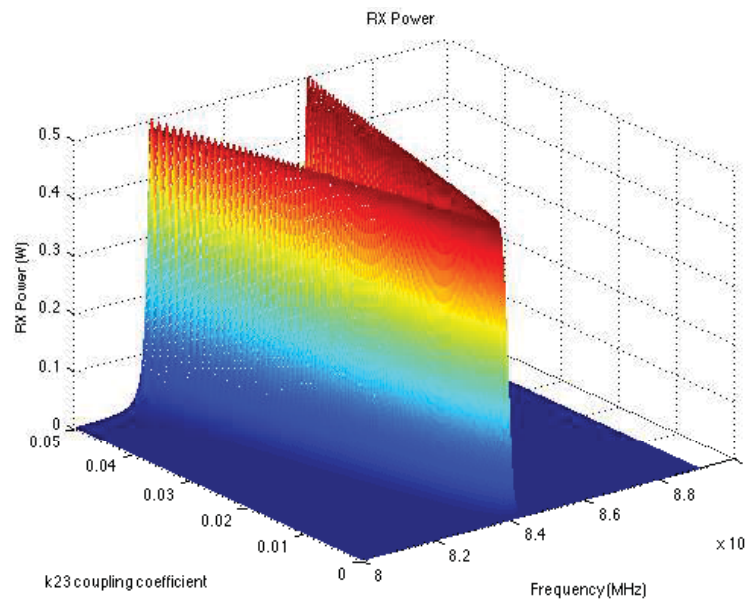

Fig. 4.3. Receive power vs. frequency and k23 coupling coefficient (distance)

The received power 3D plot with the same axis components is shown in Fig. 4.3. This is the transfer function plot that is commonly used in the wireless power transfer research community as this shows the amount of power received at varying distances. Given a 10V voltage source, the received power is maxed out at approximately 0.5W starting from the critical coupling region to the overcoupled region at a maximum k_{23} coupling coefficient of 1. Work by [17] relies on changing the source/load coil distance to their corresponding resonant coil to avoid frequency splitting while [26] employs an adjustable matching network to readjust the region to be criticially coupled. This is due to the need of a fixed source frequency. Both of these methods will adjust the region of operation to the critically coupled mode. Research by [16] however uses a frequency tracking system to adjust the source frequency to one of the resonant peaks. It would be important to point out that the efficiency seen at this resonant split frequency provides equal received power but at lower efficiencies when compared to the critically coupled mode. The power souce in this simulation is a voltage source with an unconstrained current limit which fluctutates according to the impedance seen.
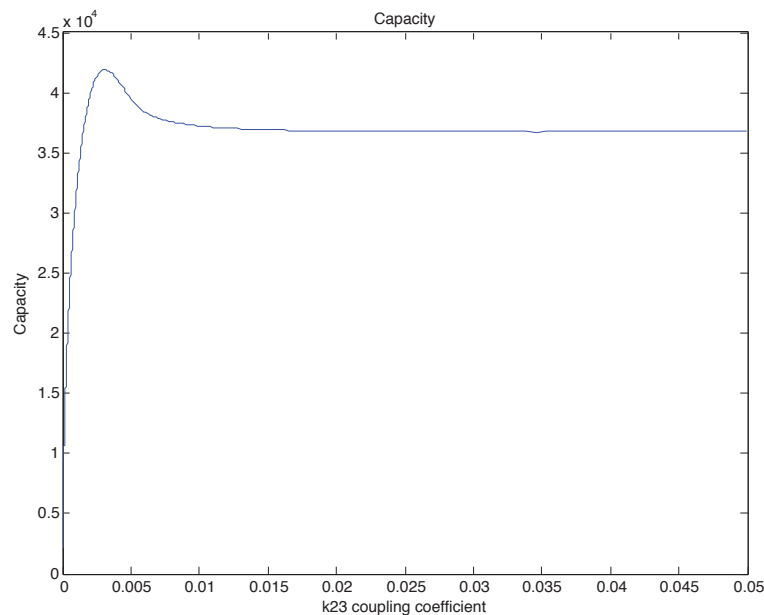

Fig. 4.4. Capacity vs. k23 coupling coefficient (distance)

Using only the total power constraint (4.8), the capacity at varying distances is studied. Simulation results in Fig. 4.4 indicate very interesting results which clearly show a peak and a plateau region where the capacity is flat. The maximum capacity peak occurs at the critically coupling point at 0.0029 and starts to flatly taper off to a coupling coefficient of 1 within the overcoupled region. Results show that to achieve maximum capacity, the system should be operating at the critically coupling point.

Fig. 4.5 describes the waterfilling power alogrithm allocation where power is prioritized to the channel with least noise. The noise power, P_N is modelled as an AWGN source with variance N_0 scaled with the efficiency function η_i as given by

$$P_{N,i} = \frac{N_0}{\eta_i}. \tag{4.15}$$

Using (4.7), the capacity can be rewritten as

$$C = \Delta_f \sum_{i=1}^{n} \log_2(1 + \frac{P_i^*}{P_{N,i}}). \tag{4.16}$$

The allocation power given a varying k_{23} coupling coefficient with respect to frequency is shown in Fig. 4.5. Fig. 4.6 describes the total available power at different frequencies and distance. The circuit model uses a fixed voltage source without a current limit which changes the available power depending on the effective load seen. The capacity simulation in (4.4) is assuming fixed power. It is important to note that the received power shown in Fig. 4.3 has an available output power that changes according to the load. To get a clearer picture at a fixed available power constraint condition, the voltage source in the simulation would have to be dynamically changed for equal power output. This is one of the reasons why methods used by [16] although simple to perform are not optimal in terms of maximing information rate and subsequently the overall efficiency of the system.
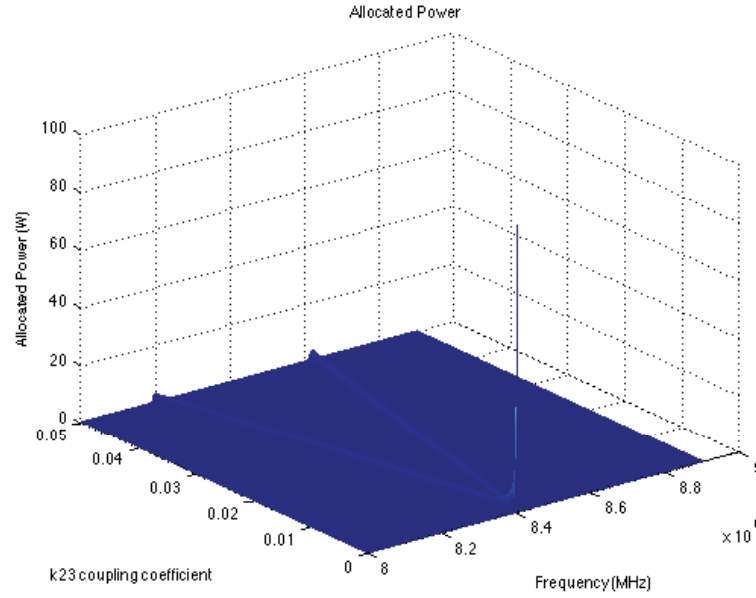
Fig. 4.5. Allocated power vs. frequency and k23 coupling coefficient (distance)
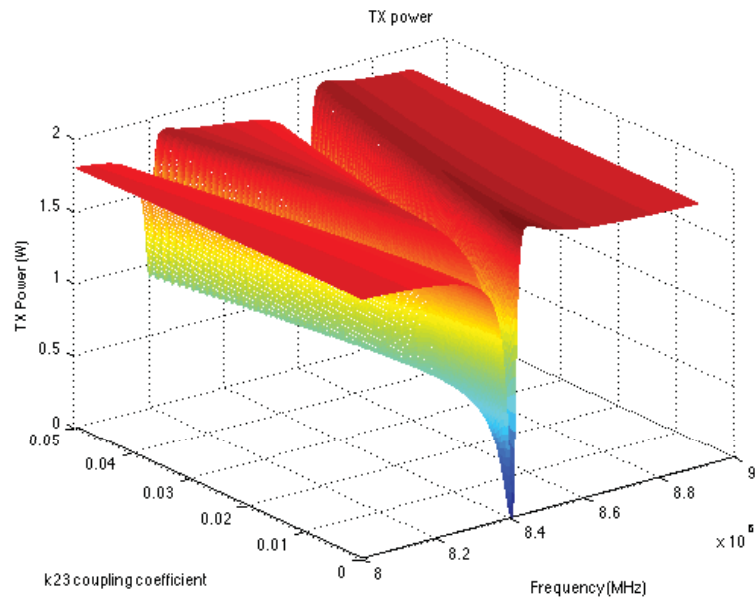
Fig. 4.6. Transmitter power vs. frequency and k23 coupling coefficient (distance)

4.4 Tradeoff analysis between information and power transfer

The simulation results shown in Section 4.3 covered the maximum information rate without regards to a constrained delivered power. Future work to analyze capacity at

different delivered power levels is of great interest. A CVX MATLAB optimization toolbox extension [40] developed by Prof. Boyd's group is a suitable candidate to analyze this data using both constraints. We have used it to verify the results shown in [36] and would prove to be useful in analyzing the tradeoffs particularly to the coupled magnetic resonance wireless power transfer method. This analysis is subject of future work.

5. SUMMARY

In this dissertation, we analyzed the practical considerations in implementing multiple transmitters for wireless power transfer via coupled magnetic resonance. The gain and diversity effect of having multiple transmitters was discussed. Transmitter resonant coupling degradation effects were shown theoretically and experimentally. The practical issues pertaining to transmitter signal synchronization in terms of frequency, phase and gain was shown. Interference scenarios such as foreign metal interaction was also discussed. The innovation of using the electrical mains for TX synchronization was devised and experimentally proven.

A novel time division multiplexing method for mitigating tightly coupled receivers in the CMR setup was proposed. The reason and solution behind the degradation effects of having tightly coupled receivers were shown mathematically and experimentally. For the setup used in this work, a 335% increase in average received power was achieved. The detuning and synchronization circuitry was explained in detail. Methods of initiating TDM and future TDM enhancements of a dynamic TDM mode and an intelligent tunable TDM was described.

The future work of analyzing the capacity seen on the CMR wireless power transfer method was simulated using parameters used in Chapters 2 and 3. It was shown that maximum capacity can be achieved at the critical coupling point of the system.

LIST OF REFERENCES

LIST OF REFERENCES

[1] R. Johari, J. Krogmeier, and D. Love,"Analysis and practical considerations in implementing multiple transmitters for wireless power transfer via coupled magnetic resonance," *IEEE Trans. Ind. Electron.*, vol. 61, no. 4, pp. 1774-1783, April 2014.

[2] K. Finkenzeller, *RFID Handbook: Fundamentals and Applications in Contactless Smart Cards, Radio Frequency Identification and Near-Field Communications*, 3rd ed., Wiley, 2010.

[3] A. Kurs, A. Karalis, R. Moffatt, J.D. Joannopoulus, P. Fisher and M. Soljacic,"Wireless Power Transfer via Strongly Coupled Magnetic Resonances," *Science*, vol. 317, pp. 83-86, July 6 2007.

[4] A. Karalis, J.D. Joannopoulus, and M. Soljacic, "Efficient wireless non-radiative mid-range energy transfer," *Ann. Phys.*, vol. 323, pp. 34-48, Jan. 2008.

[5] F. Zhang, S. Hackworth, W. Fu, C. Li, Z. Mao, and M. Sun, "Relay effect of wireless power transfer using strongly coupled magnetic resonances," *IEEE Trans. Magnetics*, vol. 47, no. 5, pp 1478-1481, May 2011.

[6] A. Kurs, R. Moffatt, and M. Soljacic, "Simultaneous mid-range power transfer to multiple devices," *Appl. Phys. Lett.*, vol. 96, p. 044102, Jan. 2010.

[7] J. Kim, H. Son, K. Kim, and Y. Park "Efficiency Analysis of Magnetic Resonance Wireless Power Transfer with Intermediate Resonant Coil," *IEEE Antennas and Wireless Prop. Letters*, Vol.10, 2011.

[8] M. Kiani, and M. Ghovanloo, "An RFID-Based Closed-Loop Wireless Power Transmission System for Biomedical Applications," *IEEE Transaction on Circuits and Systems - II: Express Briefs*, Vol. 57, no. 4,Apr. 2010.

[9] B. Cannon, J. Hoburg, D. Stancil, and S. Goldstein, "Magnetic resonant coupling as a potential means for wireless power transfer to multiple small receivers," *IEEE Trans. Power Electron.*, vol. 24, no. 7, pp. 1819-1825, July 2009.

[10] T. Imura, H. Okabe, and Y. Hori, "Basic Experimental Study on Helical Antenna of Wireless Power Transfer for Electric Vehicles by using Magnetic Resonance Couplings," *IEEE Vehicle Power and Propulsion Conf.*, Sept. 2009.

[11] D. Ahn, and S. Hong, "Effect of Coupling between Multiple Transmitters or Multiple Receivers on Wireless Power Transfer," *IEEE Trans. Ind. Electron.*, vol. 60, no. 7, July 2013.

[12] D. Ahn, and S. Hong, "A Study on Magnetic Field Repeater in Wireless Power Transfer," *IEEE Trans. Ind. Electron.*, vol. 60, no. 1, Jan. 2013.

[13] S. Cheon, Y. Kim, S. Kang, M. L Lee, J. Lee, and T. Zyung, "Circuit-model-based analysis of a wireless energy-transfer system via coupled magnetic resonances," *IEEE Trans. Ind. Electron.*, vol. 58, no. 7, pp 2906-2914, July 2011.

[14] I. Yoon and H. Ling, "Investigation of Near-Field Wireless Power Transfer Under Multiple Transmitters," *IEEE Antenna and Wireless Propagation Letters*, vol. 10, pp 662-665, June 2011.

[15] A.K. RamRakhyani, S. Mirabbasi, and M. Chiao, "Design and optimization of resonance-based efficient wireless power delivery systems for biomedical implants," *IEEE Trans. Biomed. Circuits Syst.*, vol. 5, no. 1, Feb. 2011.

[16] A. Sample, D. Meyer, and J. Smith, "Analysis, experimental results and range adaptation of magnetically coupled resonators for wireless power transfer," *IEEE Trans. Ind. Electron.*, vol. 58, no. 2, Feb. 2011.

[17] T.P. Duong, and J. Lee, "Experimental Results of High-Efficiency Resonant Coupling Wireless Power Transfer using a Variable Coupling Method," *IEEE Microwave and Wireless Component Letters*, vol. 21, no. 8, Aug. 2011.

[18] T. Imura, and Y. Hori "Maximizing Air Gap and Efficiency of Magnetic Resonant Coupling for Wireless Power Transfer Using Equivalent Circuit and Neumann Formula," *IEEE Trans. Ind. Electron*, Vol. 58, no. 10, Oct. 2011.

[19] C. Zhu, K. Liu, C. Yu, R. Ma, and H. Cheng, "Simulation and experimental analysis on wireless energy transfer based on magnetic resonances," *Proc. IEEE Vehicle Power and Propulsion Conf.*, Harbin, China, Sept. 2008.

[20] Z. N. Low, R. Chinga, R. Tseng, and J. Lin, "Design and test of a high-power high-efficiency loosely coupled planar wireless power transfer system," *IEEE Trans. Ind. Electron.*, vol. 56, no. 5, pp. 18011812, May 2009.

[21] M. Kiani, and M. Ghovanloo "The Circuit Theory Behind Coupled-Mode Magnetic Resonance-Based Wireless Power Transmission," *IEEE Trans. on Circuits and Systems*, Vol. 59, no. 8, Aug. 2012.

[22] N. Oodachi, K. Ogawa, H. Kudo, and T. Morooka "Efficiency Improvement of Wireless Power Transfer via Magnetic Resonance using Transmission Coil Array," *IEEE Symp. on Antennas and Propogation (APSURSI)*, pp. 1707 - 1710, July 2011.

[23] S. Rajagopal, and F. Khan "Multiple Receiver Support for Magnetic Resonance Based Wireless Charging," *IEEE Intl. Conf. on Communications Workshops (ICC)*, pp. 1 - 5, June 2011.

[24] J. Agbinya "Framework for Wide Area Networking of Inductive Internet of Things," *IET Electronic Letters*, Vol. 47, no. 21, Oct. 2011.

[25] W.X. Zhong, X. Liu, and S.Y. Hui "A Novel Single-Layer Winding Array and Receiver Coil Structure for Contactless Battery Charging Systems With Free-Positioning and Localized Charging Features," *IEEE Trans. on Industrial Electronics* , Vol. 58, no. 9, Sept. 2011.

[26] C. Chen, C. Lin, and Z. Jou "A Study of Loosely Coupled Coils for Wireless Power Transfer," *IEEE Trans. on Circuits and Systems - II: Express Briefs*, Vol. 57, no. 7, July. 2010.

[27] W. Lee, W. Son, K. Oh and J. Yu "Contactless Energy Transfer Systems using Antiparallel Resonant Loops," *IEEE Trans. on Industrial Electronics*, Vol. 60, no. 1 Jan. 2013.

[28] H. Ferreira, L. Lampe, J. Newbury, and T. Swart, *Power Line Communications: Theory and Applications for Narrowband and Broadband Communications over Power Lines*, 1st ed., Wiley, 2010.

[29] H.A Haus, *Waves and Fields in Optoelectronics*, Prentice Hall, 1984.

[30] Zhang, Y., Lu, T. Zhao, Z., He, F., Chen, K., and Yuan, L., "Selective Wireless Power Transfer to Multiple Loads Using Receivers of Different Resonant Frequencies," *Power Electronics, IEEE Transactions on* , vol.PP, no.99, pp.1,1

[31] Jiwariyavej, V., Imura, T., Koyanagi, T., Moriwaki, Y., Hori, Y., and Nagai, C.; Ando, K.; Watanabe, K.; Uyama, M.," Basic experimental study on effect of bentonite to efficiency of wireless power transfer using magnetic resonance coupling method," *Telecommunications Energy Conference (INTELEC), 2011 IEEE 33rd International* , vol., no., pp.1,4, 9-13 Oct. 2011

[32] Z. Low, J. Casanova, and J. Lin," A loosely coupled planar wireless power transfer system supporting multiple receivers", *Hindawi Publishing Corp., Advances in Power Electronics*, Vol. 2010, ID. 546529, March 2010.

[33] S. Rajagopal, and F. Khan, "Multiple Receiver Support for Magnetic Resonance Based Wireless Charging," *IEEE Intl. Conf. on Communications Workshops (ICC)*, pp. 1 - 5, June 2011.

[34] A4WP - alliance for wireless power. [Online]. Available: http://www.rezence.com/technology/technical-specification

[35] Qi - wireless power consortium. [Online]. Available: http://www.wirelesspowerconsortium.com

[36] P. Grover, and A. Sahai, "Shannon meets Tesla: Wireless information and power transfer," *ISIT*, pp. 2363-2367, 2010.

[37] T.M Cover and J.A Thomas, "*Elements of Information Theory*, John Wiley & Sons, 2012.

[38] Caspers, E.P., Yeung, S.H., Sarkar, T.K., Garcia-Lamperez, A., Palma, M.S.; Lagunas, M.A., Perez-Neira, A., "*Analysis of Information and Power Transfer in Wireless Communications,*" *Antennas and Propagation Magazine, IEEE*, vol.55, no.3, pp.82,95, June 2013

[39] Y. Zhang, T. Lu, Z. Zhao, F. He, K. Chen, and L. Yuan, "Selective wireless power transfer to multiple loads using receivers of different resonant frequencie," *IEEE Trans. Power Electron.*, vol. PP, no. 99, pp. 11, 2014.

[40] M. Grant, S. Boyd, and Y. Ye, "CVX: Matlab software for disciplined convex programming," [Online]. Available: http://stanford.edu/∼boyd/cvx, 2008.

[41] Varshney, L.R., Grover, P., Sahai, A.,"Securing inductively-coupled communication," *Inf. Theory and Applicat. Workshop (ITA)*, 2012 , vol., no., pp.47,53, 5-10 Feb. 2012

[42] Azad, U., Jing, H.C., Wang, Y.E.,"Link Budget and Capacity Performance of Inductively Coupled Resonant Loops," *IEEE Trans. Antennas and Propagation*, vol.60, no.5, pp.2453-2461, May 2012

VITA

VITA

Rizal Johari received his B.S. and M.S. degree from Purdue University, West Lafayette, in 2006 and 2012, respectively.

In 2006 and 2008, he was an RF Hardware Engineer with Motorola Mobile Devices at Libertyville, IL. and Singapore AMK, where he played an important role in the successful launch of the Motorola 3G RAZR and Motorola Tundra mobile phones. He spent the summer of 2013 at Apple working on next generation iPads. His research interests include wireless power transfer, software defined radio and power line communications. He is a member of Eta Kappa Nu and Tau Beta Pi.